Physics – Uspekhi **47** (5) 493 – 510 (2004)

REVIEWS OF TOPICAL PROBLEMS PACS numbers: **74.20.–z**, 74.62.Dh, **74.72.–h**

Phase diagram of $La_{2-x}M_xCuO_4$ as the key to understanding the nature of high-T_c superconductors

K V Mitsen, O M Ivanenko

DOI: 10.1070/PU2004v047n05ABEH001384

Contents

1. Introduction **493**
2. The electronic spectrum of high-T_c superconductors **494**
3. Doping and the formation of active – U centers **495**
4. Ordering of dopants **496**
5. Percolation and the phase diagram $T_c(x)$ for $La_{2-x}M_xCuO_4$ **499**
6. Generation of additional hole carriers and a mechanism for their relaxation **500**
7. Fluctuational superconductivity and the pseudogap **503**
8. Incommensurate modulation of charges and spins in $La_{2-x}M_xCuO_4$ **505**
8.1 The current situation and statement of the problem; 8.2 Parallel stripes; 8.3 Diagonal stripes; 8.4 Dynamic stripes
9. Conclusions **508**
References **509**

Abstract. Results of high-T_c superconductivity studies are analyzed using the authors' model, which assumes that the interaction of electrons with two-site negative-U centers (due to charged dopant localization near impurity ions) is responsible for many anomalous properties, and indeed the very superconductivity, of high-T_c superconductors. It is shown that the basic properties of high-T_c superconductors and the details of the superconducting and magnetic phase diagrams of $La_{2-x}M_xCuO_4$ (M = Ba, Sr) can be explained by this model.

1. Introduction

In the 17 years that have passed since the discovery of high-T_c superconductors [1] many different and mutually exclusive models have been suggested [2], models that to one extent or another explain the nature of the ground state and the anomalous properties of these compounds. However, the absence of a crucial experiment has made it impossible to choose the only correct model among the spectrum of models. Today, the most thoroughly studied high-T_c superconducting compounds are $La_{2-x}M_xCuO_4$ (M = Ba, Sr), whose phase diagram exhibits many well-reproducible features and has been thoroughly studied in the entire doping range. Hence, the results of comparisons between the experimental phase diagram of $La_{2-x}M_xCuO_4$ and the phase diagram obtained in this or that model may serve as the key argument in selecting the correct mechanism responsible for the unusual properties of high-T_c superconductors. In this article we present an elementary model of high-T_c superconductors [3], which, nevertheless, provides a good picture of the main properties of such compounds and, in particular, describes all the characteristic features of the phase diagram of $La_{2-x}M_xCuO_4$.

Here are the main ideas underlying the model:

• the doped charges in high-T_c superconductors are localized in the immediate vicinity of an impurity ion;

• as a result of such doping, negative U centers [4] ($-U$ centers), i.e., pair states on which a pair of electrons has a negative correlation energy, form on some pairs of neighboring cations;

• in the process of doping, the insulator – metal transition in high-T_c superconductors passes through the concentration range where two-electron transitions on $-U$ centers are possible, while one-electron transitions are forbidden;

• the interaction of electrons with $-U$ centers is the mechanism responsible for many anomalous properties of high-T_c superconductors, including, among other things, high-T_c superconductivity proper, carrier kinetics, the pseudogap, etc.

• this mechanism proves effective in the presence of percolation along $-U$ centers, facilitated by the ordering of ions of the doping impurity (dopant) in $La_{2-x}M_xCuO_4$;

• the ordering of the dopants in certain lattices leads to the formation of an incommensurate spin texture imitating stripe modulation [5], with the incommensurability parameter $\delta = x$ (x is the dopant concentration);

• due to the local nature of doping, a high-T_c superconductor is a spatially inhomogeneous system in which the superconducting regions coexist either with insulating regions (in underdoped samples) or with regions of a normal metal (in overdoped samples).

K V Mitsen, O M Ivanenko P N Lebedev Physics Institute, Russian Academy of Sciences
Leninskiĭ prosp. 53, 119991 Moscow, Russian Federation
Tel. (+7-095) 132 63 02. Fax (+7-095) 938 22 51
E-mail: mitsen@sci.lebedev.ru

Received 18 December 2002, revised 9 January 2004
Uspekhi Fizicheskikh Nauk **174** (5) 545 – 563 (2004)
Translated by E Yankovsky; edited by M V Magnitskaya

We will show that the 'superconducting' and magnetic phase diagrams of $La_{2-x}M_xCuO_4$ built into our model are in perfect agreement with the experimental data. We believe that such agreement between theoretical and experimental phase diagrams can be considered as proof of the validity of the proposed model of high-T_c superconductors.

2. The electronic spectrum of high-T_c superconductors

As is known, high-T_c superconductivity is observed in cuprates and bismuthates. To be more definite, we will focus on cuprates, although everything said about cuprates is applicable to bismuthates ($Ba_{1-x}K_xBiO_3$ and $BaPb_{1-x}Bi_xO_3$).

According to band theory, in underdoped cuprate high-T_c superconductors the upper antibonding band $\sigma^*_{x^2-y^2}$, formed by Cu $3d_{x^2-y^2}$ and O $2p_{x,y}$ states, is half-filled, which means that we are dealing with a metal, whose band structure and Fermi surface are those depicted in Fig. 1 (the hatched area represents filled states) [6, 7].

However, it is a fact that these compounds in an undoped state are insulators, and the reason for this is the strong electron correlation on the Cu ion that obstructs the presence of two electrons on copper (the d^{10} configuration). The electronic spectrum of the insulating phases of high-T_c superconducting compounds near the Fermi level E_F can be approximated by the model of a charge-transfer insulator [8], i.e., an insulator with a gap Δ_{ct} related to charge transfer. In this model (Fig. 2a), the empty upper Hubbard band, formed by unoccupied Cu$3d^{10}$ orbitals of copper ions in the CuO_2 plane, is separated from the filled lower Hubbard band by the repulsive energy of two electrons on copper, U_H. Inside the gap there is the filled band formed by oxygen $p_{x,y}$-orbitals. Hence, the gap Δ_{ct} in the spectrum is related to electron transfer from oxygen to the neighboring cation and amounts to about 1.5–2 eV for all high-T_c superconductors.

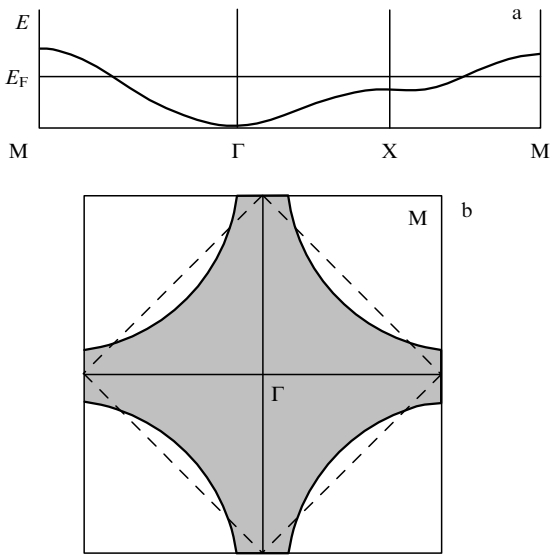

Figure 1. (a) The electronic spectrum of the CuO_2 plane predicted by band theory, and (b) the corresponding Fermi surface (the hatched area corresponds to filled states). The dashed line indicates the boundary of the Fermi surface in the tight-binding model with allowance for nearest-neighbor interaction only.

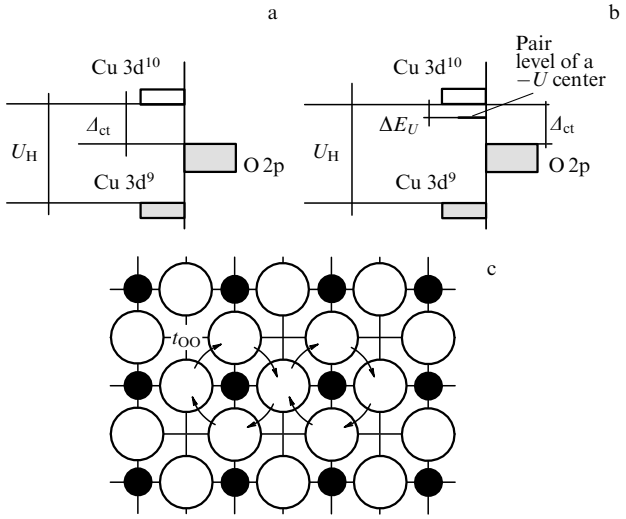

Figure 2. (a) The electronic spectrum of the insulator phase of cuprate high-T_c superconductors near E_F; (b) the same electronic spectrum with allowance for formation of a bound state of two electrons at neighboring Cu cations and two holes from the surrounding $p_{x,y}$-orbitals of oxygen ions; and (c) formation of a binding orbital of a singlet hole pair around a $-U$ center caused by the overlap of $p_{x,y}$-orbitals of oxygen (t_{OO} is the overlap integral).

Within the simple ionic model, the size of Δ_{ct} is given by the following formula [9]:

$$\Delta_{ct} \approx |\Delta E_M| + A_p - I_d \,.$$

Here I_d is the second ionization potential of copper, A_p is the electronegativity of oxygen in relation to O^{2-} formation, and $|\Delta E_M|$ is the difference in the electrostatic Madelung energies between two configurations, in one of which the given copper and oxygen ions are in states Cu^{2+} and O^{2-} and in the other in states Cu^+ and O^-. Allowing for the fact that $I_d \sim 20$ eV and $\Delta_{ct} \sim 1.5-2$ eV, we see that the balance between these three quantities is very delicate. This situation can be changed by heterovalent doping, e.g., by doping La_2CuO_4 with bivalent Ba (Sr) or by doping Nd_2CuO_4 with tetravalent Ce. What is important is that adding electrons (to Cu orbitals) or holes (to O orbitals) leads to the same result: a decrease in $|\Delta E_M|$ and, hence, in Δ_{ct}. At a certain critical concentration x_c the gap Δ_{ct} vanishes over the entire crystal and the substance becomes an ordinary metal.

This is how the ionic model explains the transition of a charge-transfer insulator into a metallic state under doping. However, we believe that in high-T_c superconducting compounds the transition from insulator to metal with increasing x passes through a special stage in which, within a certain concentration range $x_0 < x < x_c$, local two-electron transitions from oxygen ions to certain pairs of neighboring Cu cations are possible, while one-electron transitions are still forbidden.

This is possible if it is more profitable energetically to transfer two electrons from oxygen to neighboring Cu (Bi) cations via formation of a bound state (of the Heitler–London type [10]) from two electrons and two holes that emerge in the immediate vicinity of this pair of cations. In a way we end up with an intracrystalline hydrogen molecule, where the $3d^{10}$ electrons on copper act as nuclei and holes on O $2p_{x,y}$-orbitals act as electrons, with the overlap between the

orbitals (t_{OO}) creating the possibility of holes transferring from one oxygen atom to another. The analogy with an H_2 molecule is justified since the distance between cations in all high-T_c superconductors (cuprates and bismuthates) amounts to about 3.7–4.0 Å and is close to $R_0\varepsilon_\infty$, where $R_0 \approx 0.8$ Å is the distance between the nuclei in an H_2 molecule, and ε_∞ is the high-frequency dielectric constant, with $\varepsilon_\infty \approx 4.5-5$ for all high-T_c superconductors [11]. That is, nature has actually 'implanted' in high-T_c superconductors the ability to form an 'intracrystalline' hydrogen molecule. A lowering of the energy is possible, as it is in the H_2 molecule, only for the bonding orbital of a singlet hole pair. Additional lowering of the energy, ΔE_U, caused by the transition of two electrons to neighboring cations, can be estimated in the case at hand by the formula

$$\Delta E_U \sim \frac{\Delta E_{H_2}}{\varepsilon_\infty^2} \approx 0.23 \text{ eV},$$

where $\Delta E_{H_2} = 4.75$ eV is the binding energy in an H_2 molecule. If through $E(2)$, $E(1)$, and $E(0)$ we denote the energies of the ground state with, respectively, two electrons on a given pair of copper ions, one electron, and an empty pair, the above implies that $E(2) + E(0) < 2E(1)$. Thus, we can assume that a pair of neighboring copper cations in the CuO_2 plane is a $-U$ center. In other words, in the energy spectrum of a charge-transfer insulator in the case of a high-T_c superconductor there appears a pair level that is ΔE_U below the bottom of the upper Hubbard $3d^{10}$ subband (Fig. 2b).

If we now decrease Δ_{ct} to the point where the gap disappears for two-particle transitions but remains for one-particle transitions, we arrive at a system in which some of the electrons belonging to the oxygen valence band effectively interact with pair states, or $-U$ centers. We believe that the role of the doping is to activate possible $-U$ centers.

3. Doping and the formation of active $-U$ centers

It is usually assumed that in the same way as in ordinary metals, in doped high-T_c superconductors the Coulomb potential of the dopant ion is screened at a distance of about 1 Å, in view of which the distribution of doped charges in the CuO_2 plane is homogeneous. This makes it possible to assume that on the whole the electronic structure of the crystal is homogeneous. At the same time, the experiment demonstrates a pattern that is just the opposite of the one above, namely, that the doped charges are localized on a scale of an order of the lattice constant. This conclusion follows from the results of measurements of X-ray absorption fine-structure (XAFS) spectra [12] and NMR spectra [13] in $La_{2-x}Sr_xCuO_4$. Such strong localization is probably caused by the weak screening of the impurity potential in the Mott insulator [14].

We base our reasoning on the assumption that in the concentration range of interest to us ($x < 0.2$ for Ln214) and at fairly low temperatures, the doped holes (electrons) are rigidly localized in the immediate vicinity of an impurity ion. More precisely, a hole is localized in the CuO_2 plane on four oxygen ions belonging to an oxygen octahedron adjacent to a dopant ion [12, 13], while an electron is localized on four copper ions closest to a Ce ion [15] (Fig. 3).

Now, let us see how doping of local charges in a charge-transfer insulator leads to the formation of 'active' $-U$ centers. To this end, we take a fragment of the crystal structure (4a, b) that is common for all cuprates with hole doping. One such fragment is the $Cu_2R_2O_n$ cluster, where the copper ions are built into the CuO_2 plane, while the ion R = Cu in the CuO_2 plane for La_2CuO_4, R = Cu (in chains) for YBCO, and R = Bi for BSCCO. We state that in such a cluster active $-U$ centers are formed on a pair of copper ions in the CuO_2 plane, provided that at each of the oxygen octahedrons surrounding R-ions there is localized a doped hole (in YBCO and BSCCO the doped carriers are localized, respectively, around Cu ions in CuO_3 chains and around Bi in BiO planes).

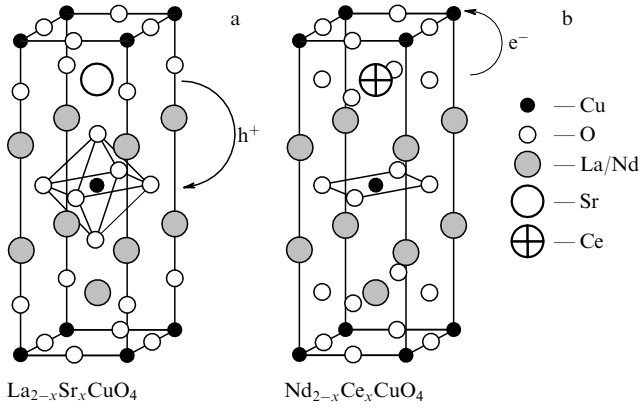

Figure 3. (a) Substitution of Sr (Ba) for La in La_2CuO_4 results in the appearance in the CuO_2 plane of a hole localized on the four oxygen ions in an oxygen octahedron adjacent to a dopant ion; (b) substitution of a Ce^{4+} ions for Nd^{3+} in Nd_2CuO_4 results in the appearance on the copper orbitals of an electron localized in the vicinity of a Ce ion.

Let us check the validity of this statement for $La_{2-x}(Ba, Sr)_xCuO_4$. Here, there can be two types of $Cu_2R_2O_n$ clusters satisfying our condition: with the distance between the R-ions (and doped holes) equal to either $3a$ or $a\sqrt{5}$, where a is the lattice constant in the CuO_2 plane. The distance between the projections on the CuO_2 plane of the corresponding dopant ions is the same.

The decrease in Δ_{ct} for Cu ions caused by the presence of a single hole near a given copper ion (Fig. 5a) can be estimated by allowing only for the interaction between the nearest neighbors and assuming that this hole is 'distributed' over the four nearest oxygen ions. The decrease in the energy of the

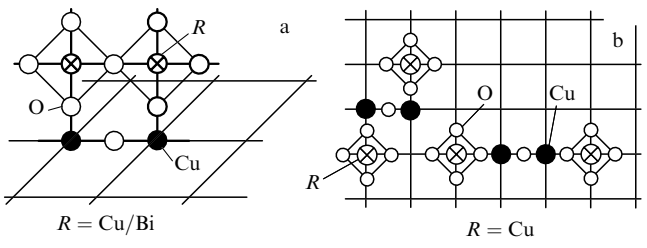

Figure 4. Atomic $Cu_2R_2O_n$ clusters common for all cuprate high-T_c superconductors with hole doping. (a) In YBCO (BSCCO), the Cu ions are built into the CuO_2 plane, and R stands for Cu (Bi) ions in CuO_3 chains (BiO planes). (b) In $La_{2-x}M_xCuO_4$ the entire cluster is built into the CuO_2 plane, and R stands for Cu ions inside the oxygen octahedron adjacent to an M ion. Two types of such clusters with a distance between the R-ions equaling $3a$ or $a\sqrt{5}$ are possible in $La_{2-x}M_xCuO_4$.

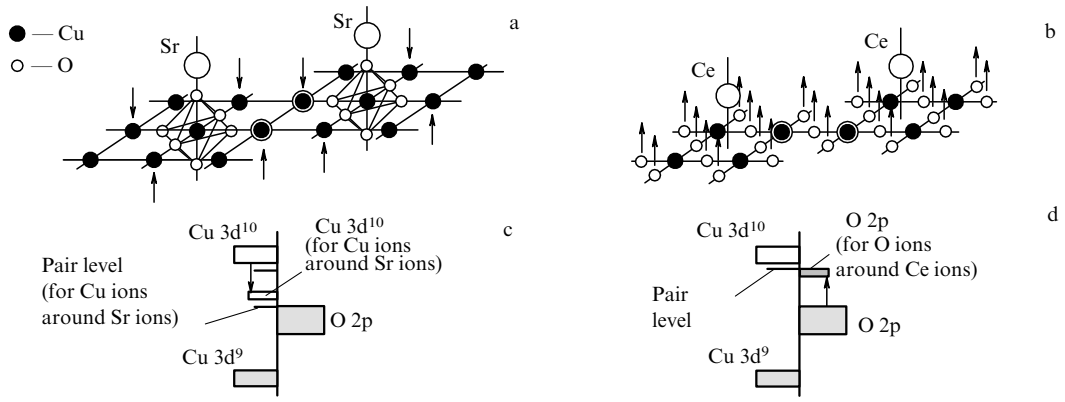

Figure 5. (a) Formation of active $-U$ centers in $La_{2-x}Sr_xCuO_4$. The arrows point to copper ions for which the energy of the Cu $3d^{10}$ state is lowered because of the presence of a doped hole localized within the oxygen octahedron. If the doped holes (or the projections of the dopants) are at a distance of $3a$ or $a\sqrt{5}$, conditions emerge for the formation of active $-U$ centers on a pair of neighboring copper ions (denoted by double circles). (b) The same for $Nd_{2-x}Ce_xCuO_4$. The arrows point to oxygen ions whose energy of the p-states is elevated because of the presence of a doped electron localized at four copper ions. (c and d) Modification of the electronic spectrum (Fig. 1b) caused by doping and accompanied by formation of active $-U$ centers for $La_{2-x}Sr_xCuO_4$ and $Nd_{2-x}Ce_xCuO_4$, respectively. Two-electron transitions from oxygen ions to a pair of neighboring copper ions become possible, while one-electron transitions are forbidden.

state Cu $3d^{10}$ for copper ions (denoted by arrows in Fig. 5a) is

$$\Delta E \approx \frac{1}{4}\,\frac{e^2}{r} \sim 1.8 \text{ eV}$$

(here, it is assumed that, being on an oxygen ion at a distance $r = a/2 \approx 2$ Å from the copper ion, the hole 'sees' the unscreened copper ion; e is the electron charge and a is the lattice constant in the CuO_2 plane). In other words, due to hole doping, the energy of these states is $\Delta E \approx 1.8$ eV below the bottom of the upper Hubbard band, which is roughly 0.1 – 0.2 eV smaller than the gap $\Delta_{ct}^0 \approx 1.9 - 2.0$ eV in undoped La_2CuO_4 (Fig. 5c).

Similarly, in $Nd_{2-x}Ce_xCuO_4$, a doped electron localized on copper orbitals in the vicinity of a Ce ion (Fig. 5b) elevates the energy of 2p-orbitals of the neighboring oxygen ions (indicated by arrows in Fig. 5b), thus lowering Δ_{ct} for the transition of an electron from these oxygen ions to the neighboring copper ions (Fig. 5d).

Thus, in both cases ($l = 3a$ and $l = a\sqrt{5}$), the presence of a doped carrier in the vicinity of each R-ion decreases Δ_{ct} for the four neighboring copper ions and creates the conditions needed for tunneling in the inner copper ions of two $p_{x,y}$-electrons from the oxygen ions surrounding this pair and the forming of a bound state with the energy lowered by $\Delta E \approx 0.23$ eV (without allowance for hybridization). Here, the emerging singlet hole pair will be localized in the vicinity of the $-U$ center.

Thus, active $-U$ centers are formed on fragments with $l = 3a$ and $l = a\sqrt{5}$, and we believe such fragments to be the nuclei of a high-T_c superconducting phase. We immediately note that in the intermediate case, where the doped holes (or the projections of the dopants) are at a distance $l = a\sqrt{8}$, no pairs of copper ions can emerge for which the vicinities of the neighboring copper cations contain doped carriers, i.e., a $-U$ center is not formed. This case corresponds to the insulating phase.

But if the doped holes are located at a distance $2a$, then for the inner copper ion the gap Δ_{ct} vanishes for one-electron transitions, too. Such a fragment is a nucleus of the metallic (nonsuperconducting) phase. At certain concentrations the entire crystal becomes a normal metal. This state corresponds to a single-band electronic spectrum in the vicinity of E_F.

Thus, doped carriers in our model are localized, and they are responsible for the formation of active $-U$ centers.

These $-U$ centers act as pair acceptors and generate additional hole pairs, which are also localized in the vicinity of the $-U$ center. Conduction occurs in such a system if these regions of localization of hole pairs form a percolation cluster in the CuO_2 plane or, in other words, if the threshold of classical percolation along $-U$ centers is exceeded.

Pair hybridization of oxygen $p_{x,y}$-states of a percolation cluster with $-U$ centers form a hybrid band, which in many ways determines the behavior of high-T_c superconductors. Electron pairing in this band, responsible for high-T_c superconductivity, emerges because of strong renormalization of the effective electron – electron interaction when scattering with intermediate virtual bound states of $-U$ centers is taken into account. Šimánek [16] was the first to propose such a mechanism, which was then repeatedly discussed in the literature as applied to various systems, including high-T_c superconductors [17 – 24].

4. Ordering of dopants

As noted earlier, the proposed mechanism of the interaction between electrons and pair states is effective when there is percolation along regions of localization of hole pairs. This, in turn, is possible only if the existing $-U$ centers form percolation clusters, which are broken lines with links whose length is $l = 3a$ or $l = a\sqrt{5}$. In the general case, where the dopant ions are randomly distributed, one can hardly expect such extended clusters to form. However, as we wish to show, in $La_{2-x}(Ba, Sr)_xCuO_4$, because of the ordering of Ba (Sr) ions, conditions emerge for the formation of percolation clusters within a broad range of dopant concentrations.

Due to the weak screening of impurity charge, the impurity ions experience mutual Coulomb repulsion. Moreover, the localization of the doped charges also presupposes the need to take into account their Coulomb repulsion at a small distance of order a, which is the lattice constant in the CuO_2 plane. This interaction increases the potential energy of

the respective impurity ions (Ba, Sr, or Ce) and also corresponds to their effective mutual repulsion. On the basis of this we can assume that in Ln214 the distance between the nearest doped charges (or, correspondingly, the projections of the dopants on the CuO_2 plane) $l \geqslant 2$ (in units of a). This corresponds to the experimentally determined solubility limit for the impurity in the parent matrix ($x_{lim} \approx 0.25$ for Ba and Sr in $La_{2-x}Sr_xCuO_4$ [1] and $x_{lim} \approx 0.2$ for Ce in $Nd_{2-x}Ce_xCuO_4$). At $x > x_{lim}$ (i.e., $l < 2$), the oxygen stoichiometry breaks down and/or there is phase separation into regions with different values of x [26–28].

The very fact that the ionic radii of Ba and Sr ($r_{Ba} \approx 1.47$ Å and $r_{Sr} \approx 1.31$ Å) are much larger than the ionic radius of La ($r_{La} \approx 1.21$ Å) [29] presupposes that the impurity ions generate a deformation field, which influences the other impurity ions. Generally, this interaction is long-range, anisotropic, and alternating, depending on the crystallographic direction [30]. One consequence of the nature of this interaction is the marked tendency of the ions (and their projections on the CuO_2 plane) to form ordered structures. Such ordering of the M ions in $La_{2-x}M_xCuO_4$ explains, in particular, the high solubility limit (x_{lim}) of Sr and Ba in La_2CuO_4 compared to that of Ce in Nd_2CuO_4, where the Ce distribution is random because $r_{Nd} > r_{Ce}$. Since the distance between the doped carriers $l \geqslant 2$, the first solubility limit ($x_{lim} \approx 0.25$) corresponds to an ordered distribution of doped charge and a close packing of circles of unit radius with a packing faction of 0.785, while the second solubility limit ($x_{lim} \approx 0.20$) corresponds to a random distribution of charges and a packing of circles of unit radius with a packing faction of 0.637 [31].

As is known (see Ref. [32]), the deformation interaction of impurities is especially strong when the impurity atoms are in interstitial positions of the lattice (interstitial impurities) and introduce large distortions into the lattice. In interstitial solid solutions, the ordered distribution of the impurity already manifests itself at very small concentrations. An estimate of the energy of the deformation interaction of impurities done in Ref. [32] shows that their ordering at low temperatures and at concentrations on the order of several atomic percentage points occurs if this energy is about 1 eV.

Let us now estimate the energy V of the deformation interaction of substitutional impurities (Ba) in the La_2CuO_4 matrix:

$$V \sim v\lambda u^2 \sim 1 \text{ eV}.$$

This value is comparable to the energy of formation of a basal crystal lattice (here, $v \sim 6 \times 10^{-23}$ cm^3 is the volume occupied by the crystal's unit cell, $\lambda \sim 2 \times 10^{12}$ erg cm^{-3} is the characteristic modulus of elasticity, and $u \sim 0.1$ is the concentration linear-expansion coefficient), which facilitates the formation of an ordered structure of dopants, beginning with low concentrations. The concentration at which Ba (Sr) ions begin to be distributed in an orderly manner depends on the way in which the crystal will be grown and thermally treated. By carefully selecting and monitoring these parameters we can guarantee that, beginning with relatively small values of x, the distribution of the dopant over La positions will be ordered. We will assume, basing our reasoning on the results of experiments, that the tendency of the dopant distribution toward becoming ordered begins at $x > 1/32$.

In addition to the deformation interaction of substitutional impurities, in antiferromagnetic (AFM) phases one must take into account the impurity-magnetic interaction [33] caused by the tendency of dopants to acquire a more profitable phase (i.e., profitable from the viewpoint of magnetic order). In high-T_c superconductors, where two-dimensional AFM correlations are observed even at $T > 1000$ K, this interaction plays an important role. Obviously, the contribution of each dopant interaction mechanism (deformation and impurity-magnetic) depends on the mobility of the dopant ion. For Ba ions, which are larger than Sr ions and hence have a lower mobility, the deformation interaction contributes the most, while for Sr ions the impurity–magnetic interactions provide a sizable contribution at fairly low concentrations, with the deformation interaction being weak.

Now let us see what ordered dopant structures (and, therefore, doped charges in the CuO_2 plane) are formed at different dopant ion concentrations if we allow only for deformation interaction. Figure 6a depicts the unit cell of La_2CuO_4, which incorporates two formula units. The La/Ba(Sr) ions occupy positions in two pairs of nonequivalent LaO planes (I–IV and II–III in Fig. 6a) separated by CuO_2 layers. Here, the La/Ba(Sr) ions occupy the sites of square sublattices shifted in relation to each other by $a/\sqrt{2}$ along the diagonal of the unit cell (a is the lattice constant).

First, we consider the distribution of Ba ions over the La positions in mirror-symmetric planes I and IV, i.e., in planes responsible for the appearance of doped charges in the central CuO_2 plane (Fig. 6a). These planes are linked by a network of oxygen octahedrons, which can transmit deformation over large distances.

As is known, in mirror planes, the substitutional impurities with a large ionic radius occupy positions in atomic networks in such a way that in each plane the occupied and vacant site complement each other. Take, for example, the picture of complete ordering at commensurate concentration $x_{com} = 1/16$ (Fig. 6b). This corresponds to the formation in each I and IV plane of square lattices with a lattice constant $L_{com} = \sqrt{32}$, and the sites of one lattice are above (below) the centers of the squares formed by the sites of the other lattice. As a result, the projections of the dopants on the CuO_2 plane (and hence the doped charges) form a square lattice with a constant $l_{com} = L/\sqrt{2} = 4$.

As the concentration grows within the interval $1/16 < x \leqslant 1/8$, the projections of the dopants may occupy positions at the centers of the squares of the lattice with $l_{com} = 4$, i.e., we can assume that within this concentration interval the free sites of the square lattice with $l_{com} = \sqrt{8}$ (Figs 6b–d) become occupied and that the fraction of occupied sites varies from 0.5 (complete 4×4 ordering) to 1 (complete $\sqrt{8} \times \sqrt{8}$ ordering). This agrees with the results of Hor and Kim [34], who observed in the IR reflection spectra of $La_{1.93}Sr_{0.07}CuO_4$ two different Goldstone modes which emerge because of translational symmetry breaking and are responsible for the formation of square lattices with the 4×4 or $\sqrt{8} \times \sqrt{8}$ type of order. In what follows, we characterize the domain in which the free sites of a square lattice with a constant l_{com} become occupied, by the corresponding value of l_{com}. In addition to domains with $l_{com} = 4$ and $\sqrt{8}$ (Figs 6b–d), the formation of completely ordered square lattices with $\sqrt{13}$, $\sqrt{10}$, 3, $\sqrt{5}$, and 2, which correspond, respectively, to

[1] In the case of $La_{2-x}Sr_xCuO_4$, special technological methods (e.g., thermal treatment in an oxygen atmosphere at high pressure) can be used to grow sufficiently uniform single crystals with $x = 0.3$ [25], which corresponds to a minimum distance $l = \sqrt{2}$ between the doped holes.

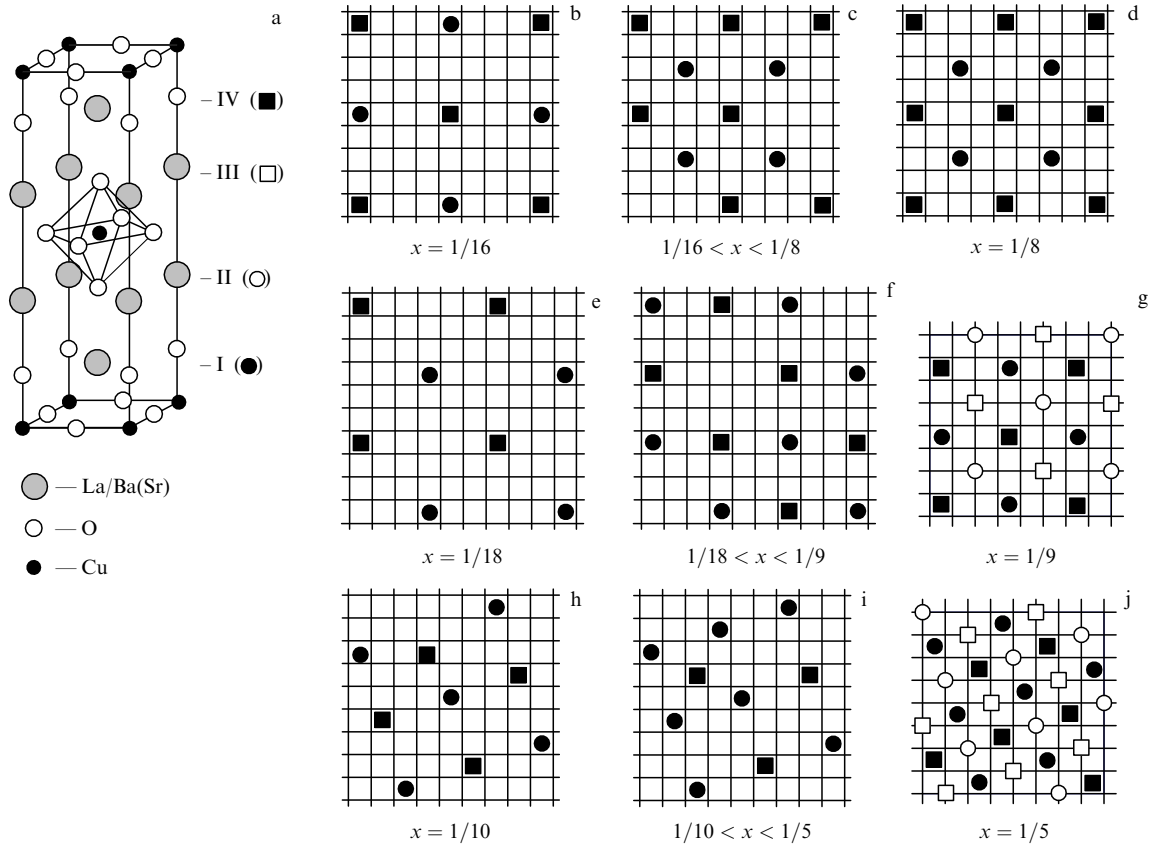

Figure 6. Types of dopant ordering in various domains. (a) The unit cell of La_2CuO_4. The roman numerals and symbols stand, respectively, for the plane number (see main text) and the ion of the dopant belonging to the given plane; (b–j) the occupation of the positions in the lattice of the dopant projections for domains with different values of l_{com} corresponding to the fraction of the occupied sites changing from 0.5 to 1; (b–d) $l_{com} = \sqrt{8}$; (e–g) $l_{com} = 3$; (h–j) $l_{com} = \sqrt{5}$; Figs. 6g and j show the projections of dopants from all the planes, I–IV.

the commensurate concentrations $x_{com} = 1/13$, $1/10$, $1/9$, $1/5$, and $1/4$, is also possible. In the case of an arbitrary value of x we assume that ordering with filling of sites of different lattices of projections with l_{com} satisfying the condition

$$\frac{1}{\sqrt{2x}} < l_{com} \leqslant \frac{1}{\sqrt{x}}$$

is possible.

This presupposes that for a given x different domains can coexist in the CuO_2 plane and that in each domain lattices with l_{com} satisfying the above condition become occupied. For instance, at $x = 1/9$ it is possible for domains to exist in which sites in a square lattice of projections with $l_{com} = \sqrt{8}$ (Fig. 6c), $\sqrt{5}$ (Fig. 6f), and $l_{com} = 3$ (Fig. 6g, complete occupancy) become occupied. As x increases, the fraction of occupied sites changes from 0.5 (at $x = 1/2l_{com}^2$) to 1 (at $x = 1/l_{com}^2$). The existence of domains with a given l_{com} is possible if the concentration satisfies the condition

$$\frac{1}{2l_{com}^2} < x \leqslant \frac{1}{l_{com}^2}\,.$$

The size of ordered domains depends on the concentration (precisely, on the proximity of x to x_{com}) and may reach 200–600 Å in the CuO_2 plane [35]. Along the c axis the size of an ordered domain is, apparently, several lattice constants due to the existence of two mirror LaO planes for each LaO plane, in view of which each type of ordering of doped charges is repeated in each second CuO_2 plane.

It is only natural that in addition to domains with an ordered distribution of dopants there are regions where the dopant distribution is disordered. As for the possibility of implementing the different types of ordering (i.e., the existence of domains with different values of l_{com}), one should expect (see Ref. [30]) that for small values of x the only domains that appear are those in which the dopants become ordered in a square lattice whose sides are parallel to the sides or diagonals of the CuO_2 cell. Hence, we assume that domains with $l_{com} = \sqrt{10}$ and $\sqrt{13}$ are not formed or, in any case, they are very small due to the possibility of different orientations in the CuO_2 plane. In view of this, the correlation length, which determines whether it is possible to observe the magnetic texture (see Section 8), is small, too. We will attribute these domains to a disordered matrix.

Thus, the $La_{2-x}M_xCuO_4$ crystal should be interpreted as a set of interpenetrating domains with different values of l_{com} determined by the concentration, and the size of these domains depends on the type of dopant and method of preparation. [2]

[2] A different ordering mechanism is also possible. For instance, the dopant ions may gather into chains along the c axis to minimize the elastic deformation energy in the ab plane. This also leads to the formation of 'cylinders of deformation' elongated along the c axis, which become ordered in a square lattice with a period depending on the dopant concentration. In this case, the threshold of percolation along the lattice sites with a period l_{com} is $x_{p0} = 0.593$ rather than 0.7, as assumed above. Accordingly, the lower limits of the concentration ranges at which percolation chains with $l = l_{com}$ can exist decrease by a factor of 1.18 [3].

5. Percolation and the phase diagram $T_c(x)$ for $La_{2-x}M_xCu0_4$

Let us now determine the threshold x_{p0} of site percolation for a square lattice with a lattice constant l_{com}. Initially only half of the sites are occupied, and such sites form a square sublattice with a constant $\sqrt{2}\,l_{com}$. One of the ways to solve this problem is to resort to the Monte Carlo method. Using a table of random numbers, we determined the percolation threshold x_{p0} for a square 32×32 lattice. Bearing in mind that initially only half of the sites were occupied, we conclude that the total fraction of occupied sites corresponding to the percolation threshold amounts to $x_{p0} = 0.70 \pm 0.01$. Table 1 lists the existence intervals and thresholds of site percolation for domains with different values of l_{com}.

Table 1. Intervals of existence and thresholds of site percolation for domains with different values of l_{com} (here, x_0 and x_M are the lower and upper limits of the range of concentrations at which the existence of domains with a given l_{com} is possible, and $x_p = x_{p0}x_M$ is the percolation threshold for a lattice with a period a when the existence of percolation chains with $l = l_{com}$ becomes possible).

l_{com}	x_0	x_p	x_M	Remarks
4	0.031	0.043	0.062	Insulator, diagonal stripes
3	0.055	0.078	0.11	High-T_c superconductor in percolation region
$\sqrt{8}$	0.062	0.087	0.125	Insulator, vertical stripes
$\sqrt{5}$	0.10	0.14	0.20	High-T_c superconductor in percolation region
2	0.125	0.175	0.25	Normal metal in percolation region

Figure 7 illustrates the percolation of localization regions of singlet hole pairs along percolation clusters with $l_{com} = 3$ (Fig. 7a) and $l_{com} = \sqrt{5}$ (Fig. 7b). Note that, as Fig. 7a shows, in the case where $l_{com} = 3$ the motion of carriers is mostly along the Cu–O bonds. This agrees with the results of Venturini et al. [36], who used IR and Raman spectroscopy data on the $La_{1.9}Sr_{0.1}CuO_4$ crystal to come to an important conclusion about such a type of motion.

Figure 8a shows the intervals of concentrations corresponding to percolation along the sites in domains with $l_{com} = 3$, $\sqrt{8}$, $\sqrt{5}$, and 2, i.e., intervals within which, according to what we have said before, there can exist broken

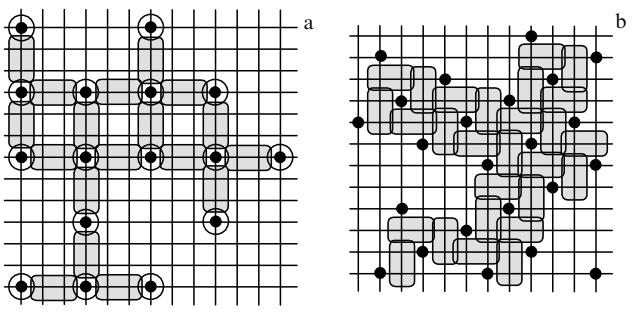

Figure 7. Percolation clusters of the localization regions of singlet hole pairs. (a) $l_{com} = 3$, and (b) $l_{com} = \sqrt{5}$. The small solid circles represent the projections of the dopant ions on the CuO_2 plane, open circles represent the regions of localization of a doped hole, and the hatched rectangles represent the localization regions of hole pairs surrounding $-U$ centers.

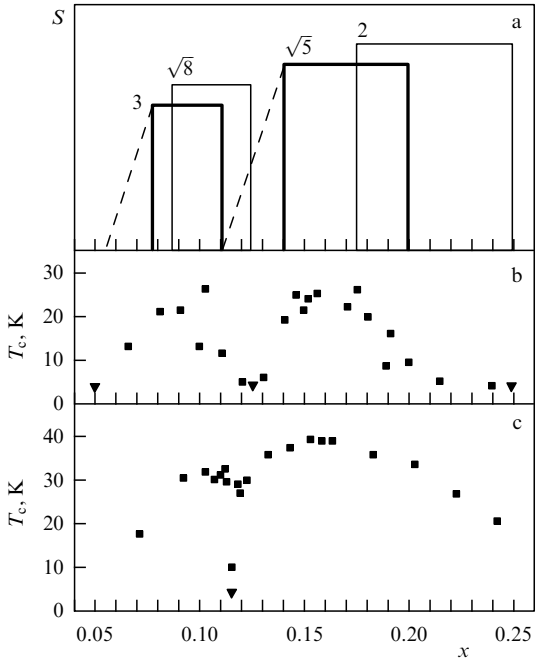

Figure 8. (a) Concentration intervals corresponding to percolation along sites in domains with $l_{com} = 3$, $\sqrt{8}$, $\sqrt{5}$, and 2. The light solid lines depict the boundaries of the regions of broken percolation lines with a link length l_{com}. The heavy solid lines depict the limits of existence of percolation clusters of $-U$ centers (i.e., broken lines with $l_{com} = 3$ and $\sqrt{5}$). The dashed straight lines limit the intervals of concentrations within which the formation of small (nonpercolation) clusters with $l_{com} = 3$ and $\sqrt{5}$ is possible. The increase in the height of each rectangle with x is a qualitative reflection of the increase in the number S of links in a percolation cluster with decreasing l_{com}; (b, c) the experimental phase diagrams $T_c(x)$ for $La_{2-x}M_xCuO_4$. The solid triangles indicate the compositions at which superconductivity was not observed down to 4.2 K: (b) $La_{2-x}Ba_xCuO_4$ [37], and (c) $La_{2-x}Sr_xCuO_4$ [38].

percolation lines with link lengths $l = \sqrt{5}$ and $l = 3$ (chains of $-U$ centers) and broken lines with $l = 2$ corresponding to a percolation cluster of the normal metal phase. Here, the solid lines depict the boundaries of the regions of broken percolation lines with a link length l_{com}. The increase in the height of each rectangle with x is a qualitative reflection of the increase in the number S of links with decreasing l_{com}. The dashed straight lines limit the intervals of concentrations within which the formation of small (nonpercolation) clusters with $l_{com} = 3$ and $\sqrt{5}$ is possible. As Fig. 8a shows, bulk superconductivity (domains with percolation chains of $-U$ centers corresponding to $l_{com} = 3$ and $\sqrt{5}$) exists within the intervals $0.077 < x < 0.11$ and $0.14 < x < 0.20$. At the same time, traces of superconductivity related to the formation of short fragments of broken lines with $l = 3$ may be observed already at $x > 0.55$. In the concentration interval from 0.175 to 0.20 superconducting domains (in which there can be percolation clusters with $l = \sqrt{5}$) and normal metal domains, with the number of the latter increasing with x, coexist. This corresponds to the transition to a state in which superconductivity is caused solely by the proximity effect, with T_c monotonically decreasing with increasing x.

The above arguments imply that at $x > 0.55$ there can be two-electron transitions to some pairs of neighboring copper ions ($-U$ centers). The transfer of electrons from oxygen ions to these $-U$ centers leads to the formation of additional hole carriers within a certain neighborhood of a $-U$ center and the

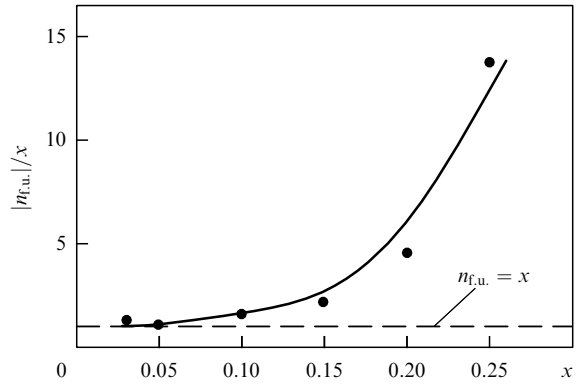

Figure 9. Dependence of the hole carrier concentration $n_{\text{f.u.}}$ (per formula unit) on x for $La_{2-x}Sr_xCuO_4$ (the data was taken from Ref. [39]).

emergence of hole conduction of the percolation type at dopant concentrations $x > x_p$ (Fig. 8a). The experiments by Plackowski and Matusiak [39] corroborate this assertion very vividly. Figure 9 shows the dependence of the hole carrier concentration $n_{\text{f.u.}}$ (per formula unit) on x for $La_{2-x}Sr_xCuO_4$. Clearly, beginning with $x > 0.05$, when, according to our model, $-U$ centers with $l = 3$ emerge, the function $n_{\text{f.u.}}(x)$ deviates from unity, which suggests that new carriers appear in addition to doped carriers. The rapid rise in $n_{\text{f.u.}}(x)$ begins at $x > 0.15$, when $-U$ centers with $l = \sqrt{5}$ begin to form.

Figures 8b and c show, for the sake of comparison, the experimental phase diagrams $T_c(x)$ for $La_{2-x}Ba_xCuO_4$ [37] and $La_{2-x}Sr_xCuO_4$ [38]. The fact that the superconductivity intervals in the experimental phase diagrams coincide with the percolation intervals for $l_{\text{com}} = \sqrt{5}$ and 3 suggests that the fragments in question, which include pairs of neighboring copper ions in the CuO_2 plane, are responsible for superconductivity in $La_{2-x}M_xCuO_4$. The same fact is an argument in favor of the proposed model of high-T_c superconductors. Note that the 'dip' in $T_c(x)$ in the interval $0.11 < x < 0.14$, caused by the absence of percolations along chains of $-U$ centers, is superimposed on the narrow region of existence (as $x \to 1/8$) of a completely ordered $\sqrt{8} \times \sqrt{8}$ lattice of doped charges, which corresponds to the insulating phase. In Section 8 we show that it is precisely this feature that makes it possible to observe a static incommensurate magnetic texture in this region [4]. The differences in the phase diagrams $T_c(x)$ for $La_{2-x}Ba_xCuO_4$ and $La_{2-x}Sr_xCuO_4$, which manifest themselves primarily in the width and depth of the 'dip', are, in our opinion, caused by the weaker deformation interaction and the higher mobility of Sr ions in comparison to Ba ions. One consequence of this is the weaker tendency of Sr ions toward ordering caused by deformation interaction.

Note that, since the sizes of the Nd and Ce ions in $Nd_{2-x}Ce_xCuO_4$ are in the reverse relation ($r_{Nd} > r_{Ce}$), there is practically no ordering of Ce. With allowance made for the fact that the minimum distance between doped electrons $l \leqslant 2$, we conclude that percolation occurs only if $x \geqslant 0.14$, and that because of the absence of ordering the percolation cluster includes both regions with $l = \sqrt{5}$ ($-U$ centers) and regions with $l = 2$ (normal metal). This agrees with the experimental phase diagram of $Nd_{2-x}Ce_xCuO_4$ [40].

Thus, we can conclude that all the features observed in phase diagrams $T_c(x)$ in $La_{2-x}M_xCuO_4$ and $Nd_{2-x}Ce_xCuO_4$ only reflect the geometrical relations in the square lattice and the competition between order and disorder in the distribution of dopant ions.

As noted earlier, the microstructure of an $La_{2-x}M_xCuO_4$ sample can be interpreted (for $x \leqslant 0.14$) as a set of clusters of $-U$ centers of different sizes immersed in an insulator matrix, with the phase volume of the latter decreasing as x increases. At high concentrations $x > 0.175$ and with the condition $l \geqslant 2$ met, the only domains that can exist are those with $l_{\text{com}} = \sqrt{5}$ and 2. Hence, true two-dimensional percolation is possible only for $x \geqslant 0.175$, while with $x < 0.175$ only three-dimensional percolation is possible (including transfer along the c axis) in combination with quantum tunneling. This agrees with the results of Ando et al. [41], who observed at $x < 0.17$ a logarithmic divergence, as $T \to 0$, in the resistivity as superconductivity was suppressed by the magnetic field.

The 'dip' in T_c in the concentration interval from 0.11 to 0.14 in $La_{2-x}Ba_xCuO_4$ is often related to a structural transformation of the low-temperature orthorhombic (LTO) phase to the low-temperature tetragonal (LTT) phase, which indeed occurs in this interval at $T = T_d > T_c$. Since in our model the 'dip' in T_c is related only to the absence in this interval of percolation clusters of $-U$ centers and the preferable presence of domains with a $\sqrt{8} \times \sqrt{8}$ order, it is advisable to also relate the LTO $\to$ LTT transformation to the 'induced' tetragonalization caused by the ordering of dopants in planes in square lattices. As shown by Phillips and Rabe [42, 43], because the Debye–Waller factor is substantially larger for Ba than for Cu or O, the interaction of Ba ions, which facilitates the formation of the LTT phase, can at low temperatures exceed the interplanar interaction, which is caused by the mismatch of different planes and facilitates the formation of the LTO phase. On the other hand, Fig. 6g shows that the given mechanism of 'induced' tetragonalization manifests itself most vividly for a completely ordered distribution of dopants at $x = 1/9$, when it becomes possible to reduce the interplanar mismatch between the BaO planes due to complete ordering of the dopants in nonequivalent positions (the planes I and II, III and IV in Fig. 6a). Hence the LTO $\to$ LTT transformation is more likely to occur at $x = 1.9$ than at $x = 1/8$. In this case, the LTT phase corresponds not to the 'dip' in T_c but, on the contrary, to a local maximum. What is interesting is that the results of the experiments conducted by Axe et al. [44], Zhou et al. [45], and Abe et al. [46] apparently corroborate this conclusion. This can serve as an indirect indication of the validity of our conclusion that the 'left' maximum of T_c in the phase diagram of $La_{2-x}Ba_xCuO_4$ is related to domains with $l_{\text{com}} = 3$. Note that the next value of the concentration at which it becomes possible to reduce the interplanar mismatch due to the complete ordering of dopants is $x = 1/5$ (Fig. 6j). And it is at this value of concentration that a transition from an LTO phase to an HTT (high-temperature tetragonal) phase occurs.

6. Generation of additional hole carriers and a mechanism for their relaxation

As is known, underdoped high-T_c superconductors with a half-filled band are insulators, although according to simple band theory, which ignores correlation effects, they should have been metals. Let us examine, in a qualitative manner, how the transition from a metallic state to an insulating state occurs when electron–electron correlations are taken into account.

Koster and Slater [47] examined the change in the band structure of a crystal caused by the injection of an isolated defect into the crystal. Their main result was that in the one-dimensional case the injection of a single defect characterized by an additional local potential U with respect to the undistorted periodic potential leads to a situation in which a single state separates from the band in question. If $U < 0$, it is the lower state that splits off, while if $U > 0$, it is the upper state that splits off. The separated state is localized in the near vicinity of the defect. Only insignificant shifts of states within the band emerge as a result, and the wave function within the band remains a delocalized Bloch function.

Now let us 'switch on' the electron–electron correlations on the copper ions one after another. We begin by increasing the potential on a single copper ion by U. Then one upper state, corresponding to a certain **k**, splits off from the half-filled band. If we 'switch on' the correlations on all copper ions, the filled states (formed primarily by oxygen orbitals) will find themselves separated from the unoccupied states (mainly copper orbitals) by a gap. As a result, on a certain contour surrounding the point M(π, π) there appears a gap Δ_{ct}, i.e., the spectrum begins to resemble that of an insulator (Fig. 10a).

If we ignore the shift of states, the electronic spectrum near E_F can be represented in the form of two bands: one filled O $2p_{x,y}$-band, whose shape in momentum space resembles that of a volcano, and one unoccupied band (shaped like a hat), formed primarily from localized Cu $3d^{10}$-orbitals. When we take into account the shift of states, the O $2p_{x,y}$-band in the insulator phase will be deformed, but the projection of the band pattern on the (k_x, k_y) plane (precisely, the contour along which the occupation number $n(k)$ diminishes substantially) for an insulator will, to a certain extent, retain the shape of the contour of the initial Fermi surface of the conductor in the absence of correlations, which follows from the fact that the boundary of the region of filled states in the direction of the point M(π, π) in the initial Fermi surface lies below the point ($\pi/2$, $\pi/2$). This follows from the results of calculations of the energy bands for the CuO_2 plane within the three-band Hubbard model [48], which takes into account the overlap of p-orbitals of the nearest oxygen atoms. As a result, the maximum band width will be in the direction of **k** along the (π, π) diagonal, i.e., along the chains of oxygen atoms, because of the overlap of oxygen $2p_x$- and $2p_y$-orbitals (the overlap integral t_{pp}), while the minimum band width of order t_{pd}^2/U (t_{pd} is the overlap integral of Cu $3d_{x^2-y^2}$ and O $2p_{x,y}$-orbitals) will be in the direction (0, π). Thus, the insulating gap will be of a d-wave nature: with a minimum along the (π, π) direction and a maximum along (0, π) and (π, 0). The above picture agrees with the results of observations of the remnant Fermi surface [49].

Under doping of $La_{2-x}Sr_xCuO_4$ (when La is replaced by Sr), the additional doped holes are localized (at least at low temperatures) in the vicinity of an impurity ion and occupy states inside the gap. As a result, the region of filled electron states diminishes as x grows, while the size of the region of hole states increases with x as $(1 + x)$.

The formation of a percolation cluster from $-U$ centers, whose pair level descends below the top of the oxygen band, opens the possibility for two-electron transitions to occur between oxygen ions and the copper ions and for two-particle hybridization of this pair level with the band states that have the highest energy to take place. This is accompanied by the restoration of the Fermi surface (or a part of this surface) in the sense of the constant-energy curve $E = E_F$ in the (k_x, k_y) plane, in which the occupation numbers $n(E)$ suddenly decrease (at $T = 0$) from 1 to 0 as E grows. However, in contrast to the Fermi surface of an ordinary metal, where for $T > 0$ electrons emerge in states with an energy $E > E_F$, in the case at hand for $T > 0$ the emerging electron pairs occupy states with an energy $E \leqslant E_F$ (Fig. 11). Accordingly, holes appear in this process along the contour of the 'restored' part of the Fermi contour.

When photoemission experiments are held for this case, a large Fermi surface of the hole type is observed. In the $La_{2-x}Sr_xCuO_4$ compound with $0.055 < x < 0.11$, due to the one-dimensional nature of the network of percolation clusters from $-U$ centers with $l = 3a$ (Fig. 7a), the excitations in the (π, π) direction are suppressed and the Fermi surface is essentially one-dimensional. At $x > 0.10$, when there is percolation along chains of $-U$ centers with $l = a\sqrt{5}$, the Fermi surface acquires a shape characteristic of the two-dimensional case (Fig. 1b).

As x increases, at $x > 0.175$ there form percolation clusters from the 'metallic' regions in which the distances between the projections of the dopants are smaller than $a\sqrt{5}$. For the states belonging to such a cluster the gap in the one-electron spectrum disappears. In this case, because tetravalent Sr replaces trivalent La, the band filling $\delta < 1/2$ and, correspondingly, the conduction is of the n-type.

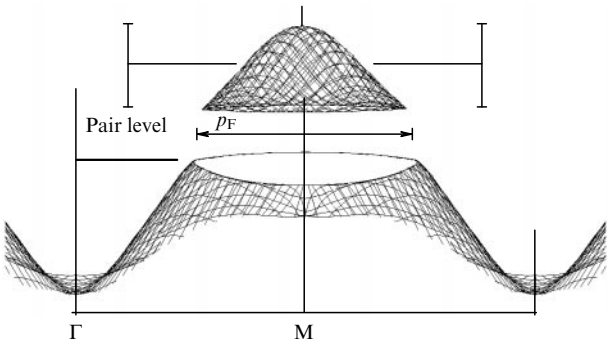

Figure 10. Dielectrization of the spectrum of the CuO_2 plane (without allowance for the shift of states) due to correlations. The upper unoccupied states are localized in the vicinity of Cu ions. The lower filled states are formed primarily from oxygen $p_{x,y}$-orbitals. The insulating gap emerges on the contour of the Fermi surface that would have existed if there were no correlations.

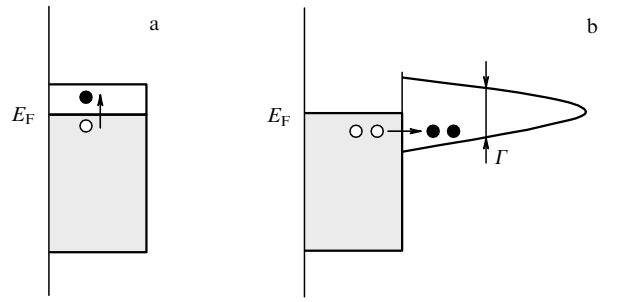

Figure 11. (a) Band structure of a normal metal; (b) band structure of a high-T_c superconductor. The holes appear in the filled band due to the transfer of electron pairs to a pair level whose width $\Gamma \propto T$.

Note that within the interval $0.055 < x < 0.11$ we have a state in which insulating and superconducting (along the percolation cluster) regions coexist, while at $x > 0.17$ there is a spatially inhomogeneous state in which normal-metal and superconducting regions coexist.

The described successive transformation of the electronic structure of $La_{2-x}Sr_xCuO_4$ with increasing x agrees well with the results of the photoemission studies of Ino et al. [50].

As a consequence of hybridization of the pair level of a $-U$ center with band states, both band and localized pair states prove to be broadened. With allowance for two-particle hybridization, the broadening of the pair level [22, 23] can be expressed as follows:

$$\Gamma \approx 4\pi kT\left(\frac{V}{E_F}\right)^2 \qquad (1)$$

(here $V \sim 1$ eV is the hybridization constant, $E_F \sim 0.5$ eV is the Fermi energy, and T is the temperature). Hence, the broadening of the pair level $\Gamma \sim (10-50)\,kT$. The corresponding broadening of band states $\gamma \propto \Gamma \propto T$.

The chemical potential of the hole pairs (measured from the position of the pair level) is always negative: $\mu_{pp} \approx -T/N$, where N is the number of hole pairs on the pair level. Since $N \gg 1$, we can assume that $\mu_{pp} \approx 0$ and coincides with the position of the pair level. Between the band and the pair level dynamic equilibrium sets in, i.e., $\mu_{pp} = \mu_p \approx 0$, where μ_p is the chemical potential of holes in the 'oxygen' band. Hence, when the pair level is at the top of the O 2p-band, the distribution of holes in the band is nondegenerate at all temperatures. Furthermore, because of the interaction with pair states, the hole distribution function differs from the Fermi one. In contrast to the latter, it varies from 1/2 to 0, not within a range of order $\sim kT$, but within an interval of order $\sim \Gamma \propto T$. However, in the photoemission spectrum, the non-Fermi nature of the hole distribution function does not manifest itself, since all the states with an energy below the top of the oxygen band are occupied by electrons, which are either in the band or on the pair level.

The occupancy η of the pair states, as well as the concentration n of holes in the oxygen band, is determined by the equality of the rates of 'band – pair level' transition and back. If N is the concentration of the $-U$ centers, then $2N\eta = n$. The rate of 'pair level – band' transitions is $N\eta\Gamma \propto T\eta$. The rate of the reverse process is determined by the electron – electron scattering frequency and is proportional to $\Gamma^2(1-\eta) \propto T^2(1-\eta)$. Thus, we arrive at the expression

$$\eta = \frac{T}{T_0 + T}\,, \qquad (2)$$

where the constant T_0 is temperature-independent. Hence, at low temperatures we have

$$n = \frac{2NT}{T_0 + T} \propto T\,,$$

which becomes a constant (equal to $2N$) at high temperatures T. This agrees with the results of measurements of the Hall effect [51, 52].

The heat capacity C_v and the magnetic susceptibility χ in such a system are determined by the hole concentration in the O 2p-band, which at low temperatures is proportional to T. For a nondegenerate (but Fermi-type) distribution, $C_v(T) = 15kn/2$ and $\chi(T) = \mu_B^2 n/kT$, where n is the carrier concentration and μ_B is the Bohr magneton [53]. In our case of a non-Fermi distribution, where the holes are created not in a layer of thickness of order $\sim kT$, measured from the top of the O 2p-band, but in a layer of thickness of order $\sim \Gamma(\propto T)$, the numerical coefficients are different, but the dependence on n and T is retained:

$$C_v(T) = \frac{\mathrm{d}}{\mathrm{d}t}\left(\int_0^\infty \varepsilon D(\varepsilon) f(\varepsilon)\,\mathrm{d}\varepsilon\right) = \frac{\mathrm{d}}{\mathrm{d}t}\left(\langle\varepsilon\rangle \int_0^\infty D(\varepsilon) f(\varepsilon)\,\mathrm{d}\varepsilon\right) = \frac{\mathrm{d}}{\mathrm{d}t}\left(\langle\varepsilon\rangle n\right) \propto T\,. \qquad (3)$$

Here, $D(\varepsilon) = \text{const}$ is the density of states in the oxygen band, $f(\varepsilon)$ is the hole distribution function (which varies from 1/2 at $\varepsilon = \mu$ to 0 at $\varepsilon > \Gamma$), and $\langle\varepsilon\rangle$ is the mean hole energy. At low temperatures, $\langle\varepsilon\rangle \sim \Gamma \propto T$ and $n \propto T$. As a result, $C_v(T) \propto T$, as in the case of a degenerate Fermi distribution. Accordingly,

$$\chi(T) = \mu_B^2 \int_0^\infty D(\varepsilon)\,\frac{\mathrm{d}f(\varepsilon)}{\mathrm{d}\varepsilon}\,\mathrm{d}\varepsilon = \frac{1}{2}\,\mu_B^2\, D = \text{const}\,. \qquad (4)$$

The deviations in the behavior of $C_v(T)$ and $\chi(T)$ at low temperatures in underdoped and overdoped samples are caused by the passage of the pair level (the chemical potential level) through the top of the O 2p-band as the doping level changes [54].

Another interesting aspect worth studying is the change in the behavior of the temperature dependence of the rate of relaxation of nuclear spin caused by doping. The results of numerous experiments show that the Korringa law $1/T_1T = \text{const}$ (where T_1 is the relaxation time for a nuclear spin in the normal state) holds in cases of underdoping and optimal doping for ^{17}O and does not hold for ^{63}Cu [55]. At the same time, in overdoped $La_{2-x}Sr_xCuO_4$ samples this law holds for ^{63}Cu, too [56]. This means that in overdoped samples, in contrast to underdoped and optimally doped samples, copper states contribute substantially to the density of electron states on the Fermi surface, which agrees with the proposed pattern of evolution of the electron states of high-T_c superconducting compounds subjected to doping.

Superconductivity in the system is caused by the effective electron – electron interaction produced by scattering processes involving intermediate virtual bound states of $-U$ centers. On the other hand, the occupancy of the $-U$ centers by electron pairs (and hence the hole concentration) decreases with temperature. Superconductivity emerges at a temperature at which the real-electron occupancy of pair states becomes low enough to ensure electron pairing because of virtual transitions of band electrons to a pair level and back. Thus, although in the normal state at $T > 0$ holes are the charge carriers, superconductivity, nevertheless, is caused by electron pairs. An indirect indication of the different signs of charge carriers participating in the normal and superconducting transport may be the change of sign of the Hall constant from plus to minus in the superconducting transition [57], while according to the classical model of Stephen and Bardeen [58], the motion of vortices should generate a Hall voltage of the same sign as in the normal state.

Thus, due to the interaction between electrons and $-U$ centers, the hole carrier distribution proves to be nondegenerate in the sense that the hole chemical potential μ is zero at all

temperatures, while degeneracy requires that μ be positive. Hence, for holes all occupation numbers are less than unity. Allowing for the nondegeneracy of the distribution (the absence of Pauli blocking) and the high hole concentration ($10^{21}-10^{22}$ cm^{-3}), we can expect that the leading contribution to relaxation processes is provided by electron–electron scattering (in our case, the scattering of hole carriers on each other). However, since the interaction of two holes in a system with $-U$ centers corresponds to effective attraction, this is not the ordinary Coulomb scattering. In the case at hand, the main electron–electron scattering mechanism is similar to the one [59] that operates in metals and alloys with strong electron–phonon interaction. In such substances, for electrons that are inside a layer of thickness $k\Theta_D$ (Θ_D is the Debye temperature) on the Fermi surface, the effective electron–electron interaction corresponding to attraction and related to the exchange of virtual phonons is much stronger than the screened Coulomb repulsion. Hence, the principal channel of electron–electron scattering in this case is also caused by the exchange of virtual phonons. The contribution of these processes [59] becomes significant when $T < \Theta_D$. Here, the electron–electron scattering amplitude does not depend on the energy E of the scattered particles at $E \ll k\Theta_D$ and rapidly decreases at $E \sim k\Theta_D$. When $E > k\Theta_D$, only the Coulomb scattering contributes to the scattering amplitude. In experiments the contribution of the electron–electron scattering to the electrical resistivity ρ ($\rho = AT^2$), exceeding the electron–phonon contribution, was observed in aluminum [60] at $T < 4$ K and in superconducting compounds with A15 structure [61] at $T < 50$ K. Here, the amplitude A exceed the value calculated on the assumption that the scattering mechanism is of the Coulomb type by a factor greater than ten.

Thus, the main contribution to the relaxation of hole carriers in high-T_c superconductors is provided by electron–electron scattering accompanied by the formation of an intermediate bound state on a $-U$ center, which can be described as the exchange of a virtual boson with an energy Ω. Since $\Omega \sim 0.2$ eV, the temperature interval where the contribution of such processes is essential extends to $T \sim 10^3$ K.

The temperature dependence $\rho(T)$ in such a model can be derived from the Drude formula

$$\rho = m^* \frac{\nu}{ne^2} ,$$

where m^* is the effective hole mass and ν is the hole carrier scattering frequency. When $\Omega \gg E$, the scattering amplitude is independent of the particle energy E. Hence, the scattering frequency ν is determined by the hole concentration and a statistical factor in the scattering cross section, i.e., the volume of the phase space available for the scattering particles, which is proportional to $E_1 + E_2$ (here E_1 and E_2 are the energies of the scattered particles measured from the band top). Hence,

$$\nu \propto n(E_1 + E_2) . \tag{5}$$

For DC conduction, $E_1 \sim E_2 \sim \Gamma \propto T$ and $\nu \propto nT \propto T^2$, with the result that $\rho(T) \propto T$. Such a dependence has been observed in experiments with optimally doped samples of $YBa_2Cu_3O_7$, $La_{2-x}Sr_xCuO_4$, $Bi_2Sr_2CaCu_2O_y$, etc.

In overdoped high-T_c superconductors, the $-U$ centers proved to be immersed in the matrix of the ordinary metal with a degenerate electron distribution. The temperature-dependent part of this resistivity in this case assumes the form

$$\rho(T) \propto \Gamma^2 \propto T^2 . \tag{6}$$

Such a dependence has been observed for various high-T_c superconductors in the 'overdoping' mode.

The predominant contribution of the electron–electron interaction to the scattering processes also has an effect on the frequency and temperature dependences of the optical conductivity σ_{opt}:

$$\sigma_{opt} = \frac{e^2 n}{m^*} \frac{\nu}{\omega^2 + \nu^2} , \tag{7}$$

where ω is the light frequency and ν is the 'optical' relaxation frequency. For electron–electron scattering (at a concentration $n \sim 10^{22}$ cm^{-3}), the collision frequency $\nu \geqslant 10^{15}$ s^{-1}. Hence, for the IR range, $\nu \gg \omega$, and the formula for the optical conductivity becomes even simpler:

$$\sigma_{opt} = \frac{e^2 n}{m^* \nu} . \tag{8}$$

For 'optical' relaxation, $E_1 \sim \omega$, $E_2 \sim \Gamma \propto T$, and $\nu \propto n\omega$ when $\omega \gg \Gamma$ and $\nu \propto nT$ when $\omega \ll \Gamma$, which suggests that $\sigma_{opt} \propto \omega^{-1}$ (for $\omega \gg \Gamma$) and $\sigma_{opt} \propto T^{-1}$ (for $\omega \ll \Gamma$). These results agree fully with the data of different experiments [62, 63].

7. Fluctuational superconductivity and the pseudogap

We will now show that our model makes it possible to explain the results of experiments on the observation of the pseudogap in high-T_c superconductors in the underdoping and optimal-doping regions. In experiments the opening of the pseudogap manifests itself in the decrease, with temperature, in the spin-lattice relaxation rate [64], the Knight shift [65], and the electronic specific heat γ [66] and the emergence of characteristic anomalies in the magnetotransport characteristics [67]. In photoemission experiments the pseudogap manifests itself in the shift of the Fermi edge. Hams et al. [68] found that a pseudogap determined in this way has the symmetry of a superconducting gap, which closes, however, at a temperature $T^* > T_c$, with T^* increasing as the hole concentration decreases.

Earlier, we assumed (see Ref. [34]) that the observed pseudogap is simply the same superconducting gap that opens, however, at $T > T_c$ as a result of large fluctuations of the number of particles caused by electron transitions between a pair level of $-U$ centers and the oxygen band. The point is that, in contrast to the ordinary superconductor with electron–phonon interaction, where the superconducting gap closes because of thermal excitations above the Fermi surface, excitations that diminish the number of states into which electron pairs can scatter, in our case it is the filling of $-U$ centers by electrons that suppresses the gap. Hence, the fluctuational decrease in the occupancy of a pair electron number facilitates the strengthening of the superconducting interaction and can lead to a fluctuational 'switching on' of superconductivity at $T^* > T > T_{c0}$ (here T_{c0} is the equilibrium value of T_c). Such large fluctuations are possible in underdoped samples, where a considerable number of the $-U$

centers belong to finite (nonpercolation) clusters. The mean size of the finite clusters decreases with the doping level, and the relative fluctuations of the occupancy of the $-U$ centers in these clusters increase in value (i.e., T^* increases). On the other hand, in 'overdoped' samples, where almost all copper ions belong to an infinite percolation cluster, large fluctuations become impossible. Using our percolation model as a starting point, we will now try to determine the dependence of the pseudogap opening temperature T^* on the doping level δ in the $YBa_2Cu_3O_{6+\delta}$ compound.

As Fig. 4a shows, in $YBa_2Cu_3O_{6+\delta}$ a $-U$ center forms in a cell if the CuO_3 chain has three filled oxygen positions in succession. The concentration of such cells with the oxygen ions in the chains being randomly distributed is δ^3. Percolation sets in when the threshold of percolation along the sites for a square lattice, which is equal to 0.593 [69], is exceeded. If we assume that such triples are distributed independently (strictly speaking, this is not the case), then $\delta_c^3 = 0.593$ and $\delta_c = 0.84$, according to the phase diagram of $YBa_2Cu_3O_{6+\delta}$ [70]. If we allow for the fact that these triples of oxygen ions are actually not distributed independently, we will find that the value of δ_c differs from 0.84, but not significantly.

For $\delta < \delta_c$, coupled $-U$ centers form clusters of various sizes. Inside each finite cluster the occupation numbers of the $-U$ centers are determined by equation (2), where the constant T_0 can be approximately found from measurements of the Hall effect [51] and varies between 400 and 800 K. In the case at hand, the inaccuracy in determining T_0 is due to the limits imposed on the range of temperature measurements (see Ref. [51]).

Let us examine a cluster in which there are S $-U$ centers. The number of electrons on the $-U$ centers in such a cluster at a temperature T is

$$N = \frac{2TS}{T + T_0} .$$

As a result of fluctuations, the number of electrons on the $-U$ centers in the given cluster can diminish by

$$\sqrt{N} = \left(\frac{2TS}{T + T_0} \right)^{1/2} .$$

The condition for fluctuation 'switching on' of superconductivity in the given cluster at the temperature T^* can be written as follows:

$$N(T^*) - \sqrt{N(T^*)} = N_c ,$$

where

$$N_c = \frac{2T_c S}{T_c + T_0}$$

is the number of electrons on the $-U$ centers at the superconducting transition point. Thus,

$$\frac{2T^* S}{T^* + T_0} - \left(\frac{2T^* S}{T^* + T_0} \right)^{1/2} = \frac{2T_c S}{T_c + T_0} . \qquad (9)$$

Solving this equation, we find T^* as a function of S. Figure 12 shows the function $T^*(S)$ for two values $T_0 = 300$ and 800 K. We see that T^* depends on T_0 very weakly. The interval of values of S is limited from the left by $S = 2$, which

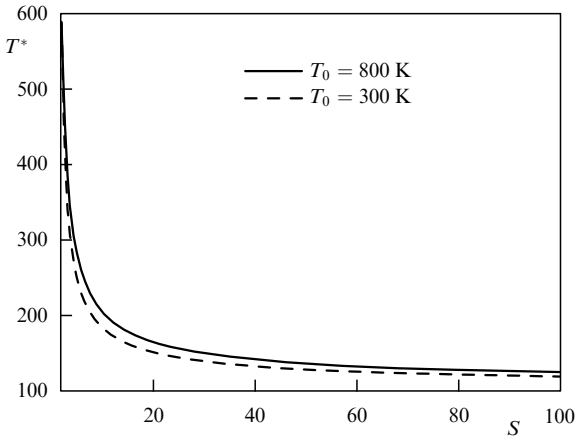

Figure 12. Dependence of the pseudogap opening temperature T^* on the cluster size S for two values of T_0.

corresponds to a cluster size of roughly 10 Å, i.e., the smallest possible superconducting region on the order of the coherence length in the CuO_2 plane.

To determine $T^*(\delta)$, we must find the mean size S of finite clusters as a function of δ. To this end, we use the results of Hu and Mak [71], who used the Monte Carlo method to study the statistics of finite clusters $S(p)$ in the problem of percolation along sites for particles with a 'hard core' on a triangular lattice with the same value of percolation threshold $p_c = 0.85$ as in our problem. Here, ρ is the probability that the given site is occupied, and p_c is the value of the probability corresponding to the percolation threshold. Along with the scaling nature of the behavior of $S(p)$ in the neighborhood of p_c [72] and the proximity of the values of the percolation thresholds in both problems, we can expect that the statistics of finite clusters in these problems are also approximately the same. Figure 13 shows the mean size S of finite clusters and the percolation probability P as functions of the probability p of site occupancy.

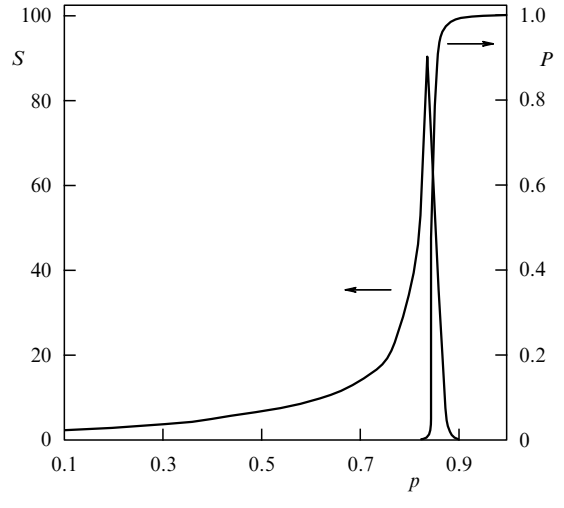

Figure 13. Dependence of the mean size S of finite clusters and the percolation probability P on the probability p of site occupancy in the problem of percolation along sites in a triangular lattice for particles with a 'hard core'.

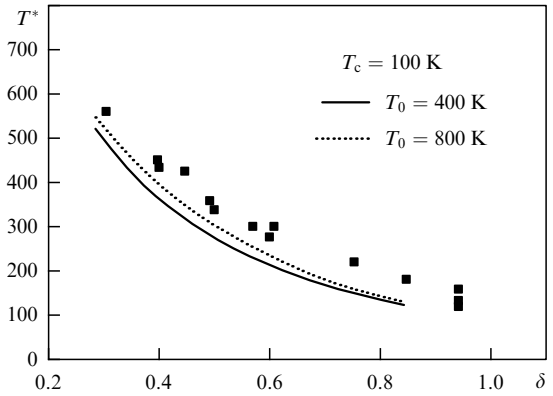

Figure 14. Calculated dependence of the pseudogap opening temperature T^* on the oxygen content δ for $YBa_2Cu_3O_{6+\delta}$. The solid squares represent the data of Ref. [73], where T^* was determined by the deviation of the temperature dependence of the resistivity from the linear one.

In the $0.1 < p < 0.82$ interval the curve $S(p)$ can be approximated with good accuracy by the dependence

$$S(p) \approx 0.9(0.95 - p)^{-2}. \qquad (10)$$

If in our problem we assume that the distribution of the excess of oxygen over the positions in the chains is random, we find that the probability p of occupancy of these positions is equal to δ. Plugging (10) into equation (9), we arrive at the dependence $T^*(\delta)$ for $YBa_2Cu_3O_{6+\delta}$, shown in Fig. 14 by a solid curve. Note that this dependence depends very weakly not only on T_0 but also on the specific shape of $S(p)$. Figure 14 shows the data from Ref. [73], where the pseudogap opening temperature was determined by measuring the deviation of the temperature dependence of resistance, $R(T)$, from the linear behavior. Even allowing for the abstract nature of such a method of determining the pseudogap opening temperature, its accuracy should be considered good. Interestingly, the minimum value of the concentration at which a pseudogap was still observed in the given experiment, $\delta = 6.3$, corresponds to $S = 2$, i.e., the smallest possible superconducting cluster.

Such fluctuational superconductivity, which emerges in microscopic regions of underdoped or optimally doped samples, is the main cause of other anomalies: fan-shaped broadening of the resistive transition [74, 75] and a jump in heat capacity [76] in a magnetic field, the anomalous Nernst effect [77], diamagnetic activity above T_c [78], the appearance of a pseudogap after irradiation of optimally doped samples, etc.

8. Incommensurate modulation of charges and spins in $La_{2-x}M_xCuO_4$

8.1 The current situation and statement of the problem

The past few years have seen many papers devoted to the study of hole-doped cuprate high-T_c superconductors that in one way or another use the concept of stripes to analyze the results of research in this field [80–91]. This concept presupposes the existence of incommensurate modulation of the spin AFM structure in the form of antiphase domains of antiferromagnetically ordered spins separated by narrow extended stripes of doped holes.

In experiments on magnetic neutron scattering, such modulation, characterized by a wave vector $\mathbf{Q}$, is observed in the form of two incommensurate peaks shifted in relation to the AFM wave vector $\mathbf{Q}_{AFM}(1/2, 1/2, 0)$ by $\varepsilon = 1/T$ along the modulation vector. Here, T is the period of the magnetic structure in units of the lattice constant. Accordingly, for charge modulation the period is $T/2$, while the related incommensurate modulation of the charge density is 2ε.

The results of neutron diffraction studies of the magnetic texture of $La_{2-x}Sr_xCuO_4$ and $La_{1.6-x}Nd_{0.4}Sr_xCuO_4$ [92–97] can be summed up in the form of a phase diagram (Fig. 15a). We see that the incommensurate elastic-scattering peaks, related to static modulation (hatched areas in Fig. 15a), are observed at Sr concentrations $x \leqslant 0.06$. In the interval $0.07 < x < 0.015$, there are incommensurate peaks in inelastic neutron scattering, which indicate the presence of dynamic modulation of the spin texture. At $x < 0.07$ there are 'diagonal' stripes with a single modulation vector directed along the orthorhombic axis b, while at $x > 0.055$ there is modulation in two directions parallel to the tetragonal axes ('parallel' stripes). In the intermediate region $0.055 < x < 0.07$ both types of modulation can be observed. To be able to compare the spin structures that appear for the cases of diagonal and parallel stripes, both types are examined in tetragonal coordinates. Here, the spin modulation incommensurability parameter $\delta = \varepsilon$ for parallel stripes and $\delta = \varepsilon/\sqrt{2}$ for diagonal stripes. For $0.03 < x < 0.12$ there exists a very simple relation (observed in experiments) between the incommensurability parameter and concentration: $\delta \approx x$.

The emergence of a stripe structure caused by the competition between electron phase separation and long-range Coulomb repulsion has been studied theoretically in

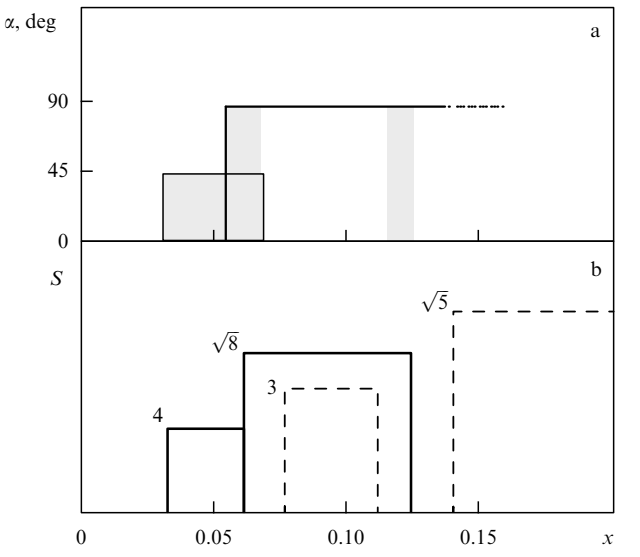

Figure 15. (a) Experimental magnetic phase diagram of $La_{2-x}Sr_xCuO_4$ [92–97]. The angle $\alpha = 45°$ corresponds to the concentration range within which diagonal stripes are observed, while $\alpha = 90°$ corresponds to the concentration range within which vertical stripes are observed. The hatched regions correspond to the regions where stationary stripes were observed. (b) The dashed lines limit the regions of percolation along $-U$ centers with $l = 3a$ and $l = a\sqrt{5}$ (dynamic stripes); the heavy lines limit the regions where $\sqrt{8} \times \sqrt{8}$ $(1/16 < x < 1/8)$ and 4×4 $(1/32 < x < 1/16)$ microdomains exist. The numbers at the vertices of the rectangles indicate the values of l_{com} for the given percolation region.

Refs [80 – 87]. An alternative mechanism of formation of an insulating 'stripe' phase in a lightly doped high-T_c superconductor due to nesting of the Fermi surface has been suggested in Refs [88 – 91]. Both theories, however, experience certain difficulties in describing the entire set of experimental results. The main ones are:

(1) the transition from diagonal stripes to parallel stripes (in LSCO) at $x \approx 0.06$;

(2) $\delta \approx x$ for $0.04 < x < 0.12$ and $\delta = \text{const}$ for $x \geqslant 0.12$;

(3) the emergence of static correlations in LSCO within a narrow region of concentrations at $x \approx 0.12$ (known as stripe pinning); and

(4) the one-dimensional nature of diagonal stripes and the two-dimensional nature of parallel stripes.

In an attempt to overcome the difficulties that appear in analyzing the results of neutron experiments, Gooding et al. [98, 99] proposed a physical spin-glass model based on the assumption that the distribution of the localized doped holes is chaotic. According to them [99], in the spin-glass phase the doped holes are localized in the CuO_2 plane. Being localized in a certain region, such a hole generates a long-range field of spin distortions. The emerging distortions of the AFM background can be described as the creation of a topological excitation, a skyrmion [100, 101], with a topological charge $Q = \pm 1$ corresponding to twisting of the AFM order parameter (Fig. 16) in the vicinity of a localized hole.

Thus, doping destroys long-range AFM order and leads to the formation of antiferromagnetically ordered disoriented microdomains whose boundaries (domain walls) are specified by localized doped holes, while the directions of AFM ordering in neighboring microdomains are turned in relation to each other through a certain angle (what is known as spin twisting). This model made it possible to explain the various features of the spin texture of $La_{2-x}Sr_xCuO_4$ observed in the spin-glass phase [102].

Below we give an alternative explanation of the observed spin and charge modulations. We use several ideas from Gooding et al. [98, 99] and combine them with our ideas concerning the mechanism of formation of $-U$ centers, dopant ordering, and percolation. To this end, we will first attempt to guess the type of spin texture (which differs from the classical stripe pattern) for some strictly ordered distributions of doped holes with $x = x_{com}$, which leads to a pattern of spin modulation that can be observed in experiments. Such an approach is justified, since we can expect the stripe model to be valid for an ordered distribution. What is more, the results of the experiment done by Fujita et al. [97] show that for $0.07 < x < 0.12$ (the region of parallel stripes), the correlation length increases from 25 Å at $x \approx 0.07$ to 200 Å at $x \approx 0.12$. It is only natural to relate the increase in the size of the correlation region to the ordering of separate AFM domains and to assume that the latter is due, in turn, to the ordering of doped holes and, correspondingly, dopant ions.

Next, we will examine how the correctly guessed texture is transformed when $x < x_{com}$ and when we deviate from the strictly ordered distribution of holes. We will then show that within a certain range of concentrations $x_p < x < x_{com}$ the main relations (which can be determined through experiments) that hold for an ideal lattice of holes at $x = x_{com}$ are conserved.

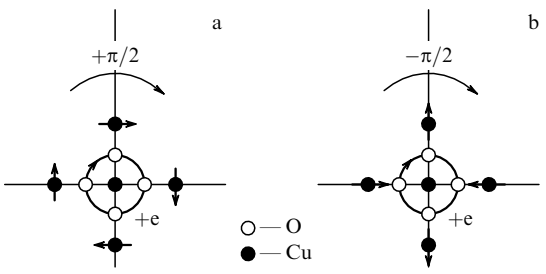

Figure 16. Rotation of the directions of spin projections on the CuO_2 plane in the vicinity of a skyrmion for topological charges $Q = 1$ (a) and $Q = -1$ (b).

8.2 Parallel stripes

Let is examine the case of complete ordering at $x_{com} = 1/8$. We assume that each hole circulates along the oxygen square surrounding a copper ion and that because of the interaction between the hole current and the spins of the four nearest copper ions the latter are polarized and the emerging distortions of the AFM background can be described as the creation of a skyrmion [100] with a topological charge ± 1 (see Fig. 16).

Figure 17a shows a possible ordering of the projections of Cu spins on the CuO_2 plane for a completely ordered arrangement of localized holes at $x = x_{com} = 1/8$, where they form a square $\sqrt{8} \times \sqrt{8}$ lattice. Here, the CuO_2 plane is broken into separate antiferromagnetically ordered tetragonal microdomains whose angles are determined by the localized doped holes. The projections on the CuO_2 plane of the directions of spins of Cu ions that are at lattice sites are indicated by arrows. The emerging consistent ordering is characterized by the AFM ordering of the microdomains and by the ordered alternation of skyrmions with charges $Q = \pm 1$. Such ordering, as Fig. 16a shows, leads to an imitation of a magnetic stripe structure. The magnetic modulation period in this case is equal to the total size of two antiphase domains along the modulation vector,

$$T = 2\sqrt{2}\, l_{com} = 8, \quad \delta = \frac{1}{8} = x, \tag{11}$$

in accordance with the experimental results. Such a picture agrees with the work by Savici et al. [103], who applied the muon spin relaxation (μsR) method to $La_{1.88}Sr_{0.12}CuO_4$ and discovered the existence of antiferromagnetically ordered microdomains (with sizes ranging from 15 to 30 Å) in which the directions of magnetization are correlated on a scale up to 600 Å. Note that, as Fig. 17a shows, in this case there are no

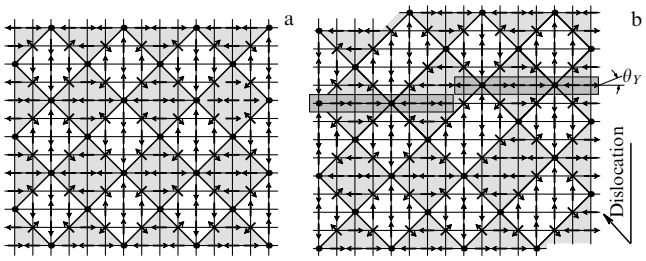

Figure 17. (a) Projections of spin directions for $x = 1/8$ when doped holes become ordered in a $\sqrt{8} \times \sqrt{8}$ lattice. The hatched areas represent the microdomains that form horizontal stripes. (b) The same as in (a) but for $x < 1/8$. The plane is broken into domains separated by diagonal dislocations. The displacement of stripes by one cell, which appears on each dislocation, leads to an effective 'tilting' of stripes through an angle θ_Y.

charge stripes in the form predicted by the theory. However, it must be said that in the case at hand we dealt with commensurate modulation which yields no satellite peaks in the diffraction patterns. Satellite reflections can appear only in the case of incommensurate modulation. Moreover, in their experiment, Tranquada et al. [92] also observed charge modulation in the form of an incommensurate splitting of the lattice peaks $(2 \pm 2\varepsilon, 0, 0)$ and $(0, 2 \pm 2\varepsilon, 0)$.

To understand why this occurs, let us go from a completely ordered lattice of doped holes at $x = 1/8$ to their distribution at $x < 1/8$. We begin by examining the experimental data gathered for the region where static parallel stripes exist at $x \approx 0.12$ [97, 104]. This gives us the possibility of comparing in detail the results of experiments with our model.

Kimura et al. [104] used an $La_{1.88}Sr_{0.12}CuO_4$ sample to observe the modulation of a spin texture with an incommensurability parameter $\delta = 0.118$. This corresponds to a mean texture period $T \approx 8.5$ (in units of a), i.e., the alternation of two periods, $T_1 = 8$ and $T_2 = 9$. Figure 17b shows the picture we proposed of an ordered distribution of doped holes (and hence of dopant projections) for a mean concentration $x = 0.118$, which was obtained by partitioning the completely ordered distribution at $x = 0.125$ along the diagonal and shifting one part in relation to the other by the vector $\mathbf{q} = (1, 1)$. Such a shift conserves the coherence of ordering in domains on both sides of the dislocation (with a small phase shift) and increases by unity the distance between neighboring parallel stripes. Actually, we introduce a diagonal dislocation with a width equal to one cell. Such a structure (Fig. 17b) produces characteristic reflections in the diffraction pattern, and these reflections correspond to incommensurate modulation of both spin (with an incommensurability parameter δ) and charge (with an incommensurability parameter 2δ). The condition of conservation of the mean concentration yields

$$T_d x_m = (T_d - 1)\, x_l\,. \tag{12}$$

In this case, T_d is the mean dislocation period in units of a, and x_l is the local concentration of holes inside a domain. To maintain the mean concentration $x_m = 0.118$ for a local concentration inside a domain $x_l = 0.125$, the introduced diagonal dislocations must have a mean period $T_d = T_1 + T_2 = 17$. Such quasiperiodic dislocations, which lead to incommensurate modulation of the crystal structure and the spin texture, guarantee the possibility of observing incommensurate reflections in diffraction experiments.

What makes the pattern of ordering so special is that, as Fig. 17b shows, the parallel stripes are shifted by one lattice constant, i.e., they can be tilted by an angle $\theta_Y = 1/17 \approx 3.3^\circ$ in relation to the tetragonal axes. It is these 'tilted' parallel stripes with a tilting angle of 3° that were observed by Kimura et al. [104].

Fujita et al. [97] studied the dependence of the angle θ_Y on the type of crystal structure in the compound $La_{1.875}Ba_{0.125-y}Sr_yCuO_4$. They found that partial substitution of Sr for Ba at $y = 0.06$ leads to a transition from the LTT phase [105] to the LTLO (low-temperature less-orthorhombic) phase. Here, the stripe tilting angle gradually changes from $\theta_Y \approx 0$ at $y = 0.05$ (in the LTT phase) to $\theta_Y \approx 2^\circ$ at $y = 0.09$ (in the LTLO phase), with $\delta \approx 0.120 \pm 0.01$ in the entire range of Sr content.

From the condition that $\delta \approx 0.120$ for all values of y it immediately follows that the mean period $T \approx 8.33$, with the period $T_d \approx 3T = 25$. Here, from equation (12) it follows that for a mean dopant concentration $x_m = 0.125$ the local dopant concentration x_l inside the domains is 0.130. This is easy to understand if we assume that a small fraction of the Sr ions (6–10%) occupies such positions in the corresponding layers (La/Ba–O) that their projections on the CuO_2 planes land at the middle points of the squares. In other words, doped holes start to fill the lattice beginning with $l_{com} = 2$, i.e., a completely ordered state (when at $x = 1/8$ the dopants occupy all positions in the $\sqrt{8} \times \sqrt{8}$ lattice) in the case of $La_{1.875}Ba_{0.125-y}Sr_yCuO_4$ is not realized in the range of concentrations y under investigation. This immediately follows from a comparison of the phase diagrams $T_c(x)$ of $La_{2-x}Ba_xCuO_4$ and $La_{2-x}Sr_xCuO_4$ (Figs 8b and c). The deep dip in $T_c(x)$ at $x = 1/8$ in $La_{2-x}Ba_xCuO_4$ compared to the small kink in $La_{2-x}Sr_xCuO_4$ suggests that in the first case the dopant ordering in a $\sqrt{8} \times \sqrt{8}$ lattice is much more complete than in the second.

If there is a preferred direction for dislocations (one of the orthorhombic axes), then at $\delta \approx 0.120$ the stripe tilting angle $\theta_Y = 1/25 \approx 2^\circ$, which corresponds to the maximum value of θ_Y observed by Fujita et al. [97] for $y = 0.085$ at the boundary between the LTLO and LTO phases. On the other hand, in the LTT phase both directions are equivalent, so dislocations in both directions that slant the stripes in opposite directions are equiprobable. As a result, the average tilting angle $\theta_Y \approx 0$ in the intermediate case where $0.05 < y < 0.09$. The angle θ_Y is determined by the predominance of dislocations of a single direction, which means that θ_Y will increase as x increases from 0.05 to 0.09.

Let us now discuss the temperature dependence of magnetic ordering and its relation to charge ordering. Fujita et al. [106] found that the emergence of long-range magnetic order (a magnetic stripe structure) is observed at temperatures T_M below the charge ordering temperature T_{ch}, which, in turn, coincides with or is below the temperature of the LTO → LTT(LTLO) transition.

As shown by Billinge et al. [107] and Haskel et al. [108, 109], the LTT–LTO–HTT transformations are of the order–disorder type in which the local tilts of the oxygen octahedrons in microdomains with a size of about 10 Å do not change and correspond to the LTT phase (rotation about the ⟨110⟩ axis). In the transformations the local LTT tilts only become more disordered with respect to each other. Since the spins are coupled to the lattice through spin–orbit coupling and through the dependence of the superexchange interaction on the octahedron tilt [110, 111], the structural disorder in the LTO phase will destroy not only charge order but also magnetic order. And vice versa, the restoration of this order as the temperature is lowered and the LTO phase transforms into the LTT or LTLO phase will successively lead to the formation first of a long-range charge order (charge stripes) and then of magnetic order (magnetic stripes) [106].

Let us now turn to the case of arbitrary values of x for $1/16 < x < 1/8$. Here, the distribution pattern can be obtained from the completely ordered distribution at $x = 1/8$ by removing a certain number of sites one after another. The texture imitating parallel stripes can emerge if a percolation cluster joining $\sqrt{8} \times \sqrt{8}$ domains into a single antiferromagnetically ordered cluster exists.

Suppose that the lattice contains such correlated remnant fragments of a parallel stripe texture genetically linked to $\sqrt{8} \times \sqrt{8}$ microdomains (Fig. 18a). The related neutron diffraction pattern exhibits characteristic reflections deter-

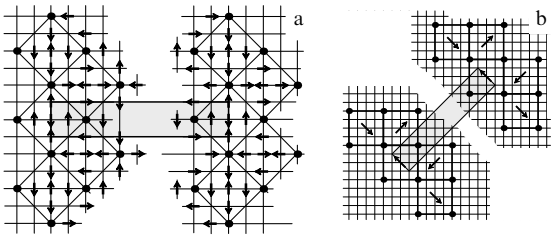

Figure 18. Fragments of a magnetic stripe texture. The texture's period, which is defined as the minimum distance between the middle points of single-phase magnetic stripes, includes two occupied sites within a band of width $l_{\rm com}/\sqrt{2}$ (hatched area). (a) Parallel stripes; the arrows indicate the directions of spin projections at each site. (b) Diagonal stripes; the arrows indicate the directions of AFM ordering in a microdomain.

mined by the mean remnant texture period. In turn, the mean period T of this texture, defined as the distance between the middle points of single-phase magnetic stripes, includes two occupied sites, as in the case of complete ordering. In other words, a rectangle with an area equal to $2T$ (hatched area in the figure) must contain two sites. This implies that

$$2Tx = 2\,, \quad \delta = \frac{1}{T} = x\,. \tag{13}$$

A sufficient condition for the above relationship to be valid is the presence of site percolation in a domain with $l_{\rm com} = \sqrt{8}$, i.e., for $0.0875 < x < 0.125$. However, at smaller values of x there can also be fairly large correlated clusters consisting of $\sqrt{8} \times \sqrt{8}$ microdomains. An exception is the interval near $x = 1/16$, where one can hardly expect that there are microdomains correlated over fairly large distances.

8.3 Diagonal stripes

Figure 19 shows an ordered distribution of the projections of copper spins at $x = 1/16$, i.e., when the doped charges are ordered in a 4×4 lattice. As in the case of $\sqrt{8} \times \sqrt{8}$ ordering, the plane is broken into antiferromagnetically ordered microdomains whose vertices are specified by localized doped holes. As a result, there forms a system of mutually perpendicular diagonal antiphase domains with a period $T = 8\sqrt{2}$ along the diagonals. Hence, $\varepsilon = 1/8\sqrt{2}$, and $\delta = 1/16$, in accordance with the experimental results.

As x decreases, in the interval $1/32 < x < 1/16$ there emerge correlated remnant fragments of a diagonal stripe texture (Fig. 17b), including 4×4 microdomains. For large domains, due to the small radius $\lambda \approx a/2$ of skyrmions on their boundary, the ordering effect of the skyrmions is not sufficient for determining the direction of ordering in the space between the stripes. While in the case of parallel stripes the direction of spin ordering in the space between stripes can be either vertical or horizontal (with an equal probability), in the case of a diagonal texture in an orthorhombic structure there is a preferred direction along the easy-magnetization axis **a**. Hence, in such fragments only one ordering direction, along **a**, is retained, and the modulation vector is directed along the other orthorhombic axis, **b**.

Repeating the same line of reasoning as for parallel stripes at $1/16 < x < 1/8$, we find that between the centers of single-phase microdomains along the modulation vector parallel to the **b** axis (precisely, in a rectangle with an area of $2\sqrt{2}T$) there are two occupied sites. In other words, $x = 1/\sqrt{2}T = \varepsilon/\sqrt{2} = \delta$, in accordance with the experimental results.

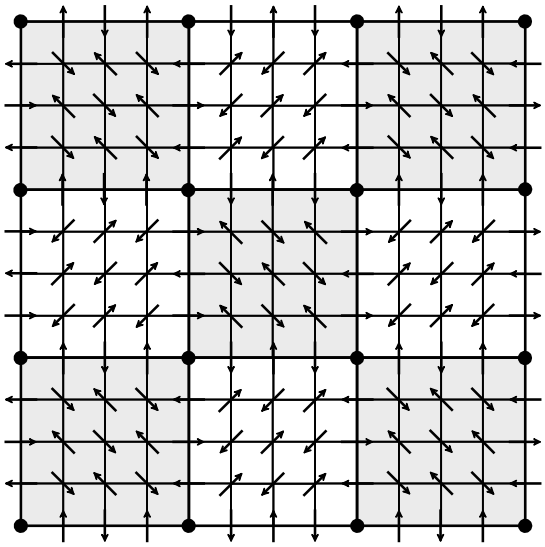

Figure 19. Projections of Cu spins in the ordering of doped holes in a 4×4 lattice.

Thus, the relation $\delta = x$ is, to a certain extent, accidental and is related to the fact that in the case of parallel stripes the occupied sites are located on lines separated by a distance of $2a$, while in the case of diagonal stripes they are located on diagonals separated by a distance of $2\sqrt{2}$. Hence, this relation is valid only in the interval $1/32 < x < 1/8$, which agrees with the experimental results.

8.4 Dynamic stripes

The last problem that we will discuss in this section deals with static and dynamic stripes. Figure 15a shows an experimental magnetic phase diagram for $La_{2-x}M_xCuO_4$ (M = Ba, Sr). Figure 15b shows the concentration ranges within which there can be antiferromagnetically correlated clusters of $\sqrt{8} \times \sqrt{8}$ microdomains for $1/16 < x < 1/8$ and 4×4 microdomains for $1/32 < x < 1/16$. The dashed lines limit the regions of existence of percolation clusters with $L = 3$ and $L = \sqrt{5}$. Such chains of doped holes in the CuO_2 plane may border on a cluster consisting of AFM microdomains. According to what we have said earlier, in regions corresponding to the existence of percolation clusters with $L = 3$ and $L = \sqrt{5}$, $-U$ centers that act as pair acceptors are formed on pairs of neighboring copper ions, and conductivity along the corresponding chains of $-U$ centers appears in these regions. This emergence of conductivity destroys the static spin correlations because of the motion of charges that disrupt the magnetic order along its path. In this case, spin correlations can be observed only in inelastic neutron scattering as dynamic incommensurate magnetic fluctuations. What is remarkable (see Fig. 15b) is that in addition to the region $x < 0.07$ there is a narrow interval of concentrations $0.11 < x < 0.125$ where there is no percolation along $-U$ centers, and it is precisely in this interval that static incommensurate correlations are again observed.

9. Conclusions

In this review we have shown that many properties of high-T_c superconductors observed in experiments have a natural explanation in the framework of the model we proposed. We believe that under doping the transition from the

insulating state to the metallic state passes through a certain concentration range, where electron pairs can go over from oxygen ions to the two neighboring copper cations, while one-electron transitions are still forbidden. It is this concentration range that corresponds to the region of high-T_c superconductivity, where the electron–electron attraction is caused by the scattering of electron pairs on $-U$ centers. Doped charges are localized, and their role is reduced to the formation of $-U$ centers. The transition of electron pairs from the oxygen band to the $-U$ centers results in the generation of additional carriers localized near the $-U$ centers. Conductivity appears in the system as a result of percolation along $-U$ centers, precisely, along the orbitals of singlet hole pairs, which is facilitated by the ordering of the dopant ions. Two-particle hybridization of a pair level and states of the oxygen band leads to dramatically new properties of the system (nondegenerate distribution of hole carriers and the predominant contribution of electron–electron scattering to energy relaxation processes), which determine the unusual behavior of high-T_c superconductors in the normal state. We have found that the ordering of the dopant ions in certain lattices also leads to the formation of an incommensurate spin texture, which imitates stripe modulation, with an incommensurability parameter $\delta = x$.

We have used the proposed model to provide a detailed explanation of the superconducting and magnetic phase diagrams of $La_{2-x}M_xCuO_4$ and have shown that the features of the phase diagrams only reflect the geometrical relations existing in a square lattice and the competition of different types of dopant ordering. The good agreement between the calculated phase diagrams and the experimental results may serve as an important argument in favor of the proposed model of high-T_c superconductors.

The authors are grateful for the support provided by the Ministry of Industry, Science and Technology of the Russian Federation (Federal Program of Theoretical and Experimental Studies of High-T_c Superconductivity Mechanisms).

References

1. Bednorz J G, Müller K A *Z. Phys. B* **64** 189 (1986)
2. Ginzburg V L, Maksimov E G *Physica C* **235–240** 193 (1994)
3. Mitsen K V, Ivanenko O M *Zh. Eksp. Teor. Fiz.* **118** 666 (2000) [*JETP* **91** 579 (2000)]
4. Anderson P W *Phys. Rev. Lett.* **34** 953 (1975)
5. Tranquada J M et al. *Phys. Rev. B* **54** 7489 (1996)
6. Mazin I I et al. *Pis'ma Zh. Eksp. Teor. Fiz.* **46** (Suppl.) 120 (1987) [*JETP Lett.* **46** (S1) S101 (1987)]
7. Mattheiss L F *Phys. Rev. Lett.* **58** 1028 (1987)
8. Zaanen J, Sawatzky G A, Allen J W *Phys. Rev. Lett.* **55** 418 (1985)
9. Mazumbar S *Solid State Commun.* **69** 527 (1989)
10. Heitler W, London F *Z. Phys.* **44** 455 (1927)
11. Harshman D R, Mills A P (Jr.) *Phys. Rev. B* **45** 10684 (1992)
12. Polinger V, Haskel D, Stern E A, cond-mat/9811425
13. Hammel P C et al. *Phys. Rev. B* **57** R712 (1998)
14. Wang Z et al. *Phys. Rev. B* **65** 064509 (2002)
15. Hirsch J E *Physica C* **243** 319 (1995)
16. Šimánek E *Solid State Commun.* **32** 731 (1979)
17. Ting C S, Talwar D N, Ngai K L *Phys. Rev. Lett.* **45** 1213 (1980)
18. Schüttler H-B, Jarrell M, Scalapino D J *Phys. Rev. Lett.* **58** 1147 (1987)
19. Yu J et al. *Phys. Lett. A* **122** 203 (1987)
20. Volkov B A, Tugushev V V *Pis'ma Zh. Eksp. Teor. Fiz.* **46** 193 (1987); **49** 337 (1989) [*JETP Lett.* **46** 245 (1987); **49** 384 (1989)]
21. Eliashberg G M *Pis'ma Zh. Eksp. Teor. Fiz.* **46** (Suppl) 94 (1987) [*JETP Lett.* **46** (S1) S81 (1087)]
22. Kulik I O *Fiz. Nizk. Temp.* **13** 879 (1987) [*Sov. J. Low Temp. Phys.* **13** 505 (1987)]
23. Arseev P I *Zh. Eksp. Teor. Fiz.* **101** 1246 (1992) [*Sov. Phys. JETP* **74** 667 (1992)]
24. Ranninger J, Robin J M *Physica C* **253** 279 (1995)
25. Nakamae S et al. *Phys. Rev. B* **68** 100502(R) (2003)
26. Radaelli P G et al. *Phys. Rev. B* **49** 4163 (1994)
27. Yoshimura K et al. *J. Phys. Soc. Jpn.* **62** 1114 (1993)
28. Paulus E F et al. *Solid State Commun.* **73** 791 (1990)
29. Shannon R D *Acta Cryst. A* **32** 751 (1976)
30. Khomskii D I, Kugel K I *Europhys. Lett.* **55** 208 (2001)
31. Ziman J M *Models of Disorder. The Theoretical Physics of Homogeneously Disordered Systems* (Cambridge: Cambridge Univ. Press, 1979) [Translated into Russian (Moscow: Mir, 1982)]
32. Khachaturyan A G *Teoriya Fazovykh Prevrashcheniĭ i Struktura Tverdykh Rastvorov* (Theory of Structural Transformations in Solids) (Moscow: Nauka, 1974) [Translated into English (New York: Wiley, 1983)]
33. Nagaev É L *Usp. Fiz. Nauk* **165** 529 (1995) [*Phys. Usp.* **38** 497 (1995)]
34. Hor P H, Kim Y H *J. Phys.: Condens. Matter* **14** 10377 (2002); cond-mat/0112250
35. Koyama Y et al. *Phys. Rev. B* **51** 9045 (1995)
36. Venturini F et al. *Phys. Rev. B* **66** 060502(R) (2002)
37. Moodenbaugh A R et al. *Phys. Rev. B* **38** 4596 (1988)
38. Kumagai K et al. *J. Supercond.* **7** 63 (1994)
39. Plackowski T, Matusiak M *Phys. Rev. B* **60** 14872 (1999)
40. Takagi H, Uchida S, Tokura Y *Phys. Rev. Lett.* **62** 1197 (1989)
41. Ando Y et al. *Phys. Rev. B* **56** R8530 (1997)
42. Phillips J C, Rabe K M *Phys. Rev. B* **44** 2863 (1991)
43. Phillips J C *Phys. Rev. B* **47** 2944 (1993)
44. Axe J D et al. *Phys. Rev. Lett.* **62** 2751 (1989)
45. Zhou F et al., cond-mat/0212282
46. Abe Y et al. *Phys. Rev. B* **59** 14753 (1999)
47. Koster G F, Slater J C *Phys. Rev.* **95** 1167 (1954)
48. Markiewicz R S *J. Phys. Chem. Solids* **58** 1179 (1997)
49. Ronning F et al. *Science* **282** 2067 (1998)
50. Ino A et al. *Phys. Rev. B* **65** 094504 (2002)
51. Ong N P et al. *Physica C* **185–189** 34 (1991)
52. Kapitulnik A *Physica C* **153–155** 520 (1988)
53. Ansel'm A I *Vvedenie v Teoriyu Poluprovodnikov* (Introduction to Semiconductor Theory) (Moscow: Nauka, 1978) [Translated into English (Moscow: Mir Publ., 1981)]
54. Levin G A, Quader K F *Physica C* **258** 261 (1996)
55. Hammel P C et al. *Phys. Rev. Lett.* **63** 1992 (1989)
56. Imai T et al. *Physica C* **162–164** 169 (1989)
57. Rice J P et al. *Phys. Rev. B* **46** 11050 (1992)
58. Stephen M J, Bardeen J *Phys. Rev. Lett.* **14** 112 (1965)
59. MacDonald A H *Phys. Rev. Lett.* **44** 489 (1980)
60. Garland J C, Bowers R *Phys. Rev. Lett.* **21** 1007 (1968)
61. Gurvitch M et al. *Phys. Rev. Lett.* **41** 1616 (1978)
62. Tanner D B et al. *J. Supercond.* **8** 563 (1995)
63. Schlesinger Z et al. *Phys. Rev. B* **41** 11237 (1990)
64. Alloul H, Ohno T, Mendels P *Phys. Rev. Lett.* **63** 1700 (1989)
65. Yasuoka H, Imai T, Shimizu T, in *Strong Correlation and Superconductivity*: *Proc. of the IBM Japan Intern. Symp., Mt. Fuji, Japan, 21–25 May 1989* (Springer Ser. in Solid-State Sciences, Vol. 89, Eds H Fukuyama, S Maekawa, A P Malozemoff) (Berlin: Springer-Verlag, 1989) p. 254
66. Loram J W et al. *Physica C* **282–287** 1405 (1997)
67. Wuyts B, Moshchalkov V V, Bruynseraede Y *Phys. Rev. B* **53** 9418 (1996)
68. Harris J M et al. *Phys. Rev. B* **54** R15665 (1996)
69. Ziff R M *Phys. Rev. Lett.* **69** 2670 (1992)
70. Beyers R et al. *Nature* **340** 619 (1989)
71. Hu C-K, Mak K-S *Phys. Rev. B* **39** 2948 (1989)
72. Shklovskiĭ B I, Efros A L *Elektronnye Svoĭstva Legirovannykh Poluprovodnikov* (Electronic Properties of Doped Semiconductors) (Moscow: Nauka, 1979) [Translated into English (Berlin: Springer-Verlag, 1984)]
73. Wuyts B, Moshchalkov V V, Bruynseraede Y *Phys. Rev. B* **53** 9418 (1996)
74. Oh B et al. *Phys. Rev. B* **37** 7861 (1988)
75. Suzuki M, Hikita M *Phys. Rev. B* **44** 249 (1991)
76. Salamon M B et al. *Phys. Rev. B* **38** 885 (1988)
77. Xu Z A et al. *Nature* **406** 486 (2000)

78. Iguchi I, Yamaguchi T, Sugimoto A *Nature* **412** 420 (2001)
79. Vobornik J et al. *Phys. Rev. B* **61** 11248 (2000)
80. Zaanen J, Gunnarsson O *Phys. Rev. B* **40** 7391 (1989)
81. Poilblanc D, Rice T M *Phys. Rev. B* **39** 9749 (1989)
82. Kivelson S A, Emery V J, Lin H Q *Phys. Rev. B* **42** 6523 (1990)
83. Schulz H J *Phys. Rev. Lett.* **64** 1445 (1990)
84. Inui M, Littlewood P B *Phys. Rev. B* **44** 4415 (1991)
85. An G, van Leeuwen J M J *Phys. Rev. B* **44** 9410 (1991)
86. Emery V J, Kivelson S A *Physica C* **209** 597 (1993)
87. Castellani C, Di Castro C, Grilli M *Phys. Rev. Lett.* **75** 4650 (1995)
88. Si Q et al. *Phys. Rev. B* **47** 9055 (1993)
89. Tanamoto T, Kohno H, Fukuyama H *J. Phys. Soc. Jpn.* **63** 2739 (1994)
90. Markiewicz R S *Phys. Rev. B* **56** 9091 (1997)
91. Belyavsky V I, Kopaev Yu V *Phys. Lett. A* **287** 152 (2001)
92. Tranquada J M et al. *Phys. Rev. B* **54** 7489 (1996)
93. Yamada K et al. *Phys. Rev. B* **57** 6165 (1998)
94. Yamada K et al. *Physica C* **282 – 287** 85 (1997)
95. Matsuda M et al. *Phys. Rev. B* **65** 134515 (2002)
96. Fujita M et al. *Phys. Rev. B* **65** 64505 (2002)
97. Fujita M et al. *Phys. Rev. B* **66** 184503 (2002)
98. Gooding R J, Salem N M, Mailhot A *Phys. Rev. B* **49** 6067 (1994)
99. Gooding R J et al. *Phys. Rev. B* **55** 6360 (1997)
100. Belavin A A, Polyakov A M *Pis'ma Zh. Eksp. Teor. Fiz.* **22** 503 (1975) [*JETP Lett.* **22** 245 (1975)]
101. Gooding R J *Phys. Rev. Lett.* **66** 2266 (1991)
102. Keimer B et al. *Phys. Rev. B* **46** 14034 (1992)
103. Savici A T et al. *Phys. Rev. B* **66** 14524 (2002)
104. Kimura H et al. *Phys. Rev. B* **61** 14366 (2000)
105. Koyama Y et al. *Phys. Rev. B* **51** 9045 (1995)
106. Fujita M et al. *Phys. Rev. Lett.* **88** 167008 (2002)
107. Billinge S J L, Kwei G H, Takagi H *Phys. Rev. Lett.* **72** 2282 (1994)
108. Haskel D et al. *Phys. Rev. Lett.* **76** 439 (1996)
109. Haskel D et al. *Phys. Rev. B* **61** 7055 (2000)
110. Bonesteel N E, Rice T M, Zhang F C *Phys. Rev. Lett.* **68** 2684 (1992)
111. Thio T et al. *Phys. Rev. B* **38** 905 (1988)